Physics of Living Systems

Optical mapping of ground reaction force dynamics in freely behaving *Drosophila melanogaster* larvae

Reviewed Preprint

Revised by authors after peer review.

About eLife's process

Reviewed preprint version 2
February 22, 2024 (this version)

Reviewed preprint version 1
July 13, 2023

Sent for peer review
April 2, 2023

Posted to preprint server
December 17, 2022

Jonathan H. Booth, Andrew T. Meek, Nils M. Kronenberg, Stefan R. Pulver, Malte C. Gather

SUPA, School of Physics and Astronomy, University of St Andrews, Fife, United Kingdom • Humboldt Centre for Nano- and Biophotonics, Department of Chemistry, University of Cologne, Germany; • School of Psychology and Neuroscience, University of St Andrews, Fife, United Kingdom

Abstract

During locomotion, soft-bodied terrestrial animals solve complex control problems at substrate interfaces, but our understanding of how they achieve this without rigid components remains incomplete. Here, we develop new all-optical methods based on optical interference in a deformable substrate to measure ground reaction forces (GRFs) with micrometre and nanonewton precision in behaving *Drosophila* larvae. Combining this with a kinematic analysis of substrate interfacing features, we shed new light onto the biomechanical control of larval locomotion. Crawling in larvae measuring ~1 mm in length involves an intricate pattern of cuticle sequestration and planting, producing GRFs of 1-7 μN. We show that larvae insert and expand denticulated, feet-like structures into substrates as they move, a process not previously observed in soft bodied animals. These 'protopodia' form dynamic anchors to compensate counteracting forces. Our work provides a framework for future biomechanics research in soft-bodied animals and promises to inspire improved soft-robot design.

eLife assessment

This study reports **important** findings about new locomotory dynamics of crawling Drosophila larva based on imaging the reaction forces during larval crawling. The evidence with the new high-resolution microscopy method is **compelling**, as it significantly improves the spatial, temporal, and force resolution compared to previous methods for studying Drosophila larva and could be applied to other crawling organisms. The manuscript explains the new technology, WARP microscopy, and provides analysis of the data to characterize small animal behavior and discover new crawling-associated anatomical features and motor patterns. The work will be of interest to the broad neuroscience community interested in the mechanisms of locomotion in a highly tractable model.

Introduction

Locomotion is a fundamental behaviour in the Animal Kingdom. There is great diversity in how it is accomplished, from the modification of torque angles in rigid bodied animals (1) to a diverse array of peristalses in limbed (2) and limbless soft-bodied animals (3). Key to these different strategies is one unifying characteristic: action against a substrate or fluid produces forces, thereby translating the body in space. In an aquatic environment, forces acting within fluids can be visualised via the waves of distortion they cause, thus facilitating the development of detailed theories of movement (4). In terrestrial settings, however, substrates are often rigid and therefore prevent direct visualisation of the ground reaction forces (GRFs) generated by animals.

Interactions with substrates have been extensively studied in animals with articulating skeletons (i.e. rigid bodied animals) due to the ability to calculate output forces from lever physics combined with measurements of joint-angles(1,5). However, much less is known about substrate interactions and GRFs in soft-bodied animals without rigid internal or external skeletons. These animals lack articulating joints upon which muscles act, ambiguating points through which the animal interacts with the substrate. However, they too must anchor a part of their body when another part is in motion to prevent net progression being impeded by an equal but opposite reaction force, i.e. their movements must obey Newton's 3rd law of motion (6). Furthermore, soft bodies pose a difficult control problem owing to their highly non-linear physical properties and virtually unlimited degrees of freedom. Movement over terrain therefore presents a unique challenge for soft animals. Dynamic anchoring has long since been postulated to be at the heart of soft-bodied locomotion (7), but understanding the mechanisms by which soft animals achieve this remains an open problem. Prior work on caterpillars (2,8–10), leeches (11,12) and *C. elegans* (13,14) provided key insights and have provided foundational observations for the inspiration of soft robot design; however, a lack of methods with sufficient spatiotemporal resolution for measuring GRFs in freely behaving animals has limited progress.

However, in the field of cellular mechanobiology, many new force measuring techniques have been developed which allow measurement of comparatively small forces from soft structures exhibiting low inertia (15–17) often with relatively high spatial-resolution. Early methods such as atomic force microscopy required the use of laser-entrained silicon probes to make contact with a cell of interest (15). This approach is problematic for studying animal behaviour due to the risk of the laser and probe influencing behaviour. Subsequently, techniques have been developed which allow indirect measurement of substrate interactions. One such approach is Traction Force Microscopy (TFM) in which the displacement of fluorescent markers suspended in a material with known mechanical properties relative to a 0-force reference allows for indirect measurement of horizontally aligned traction forces (17–19). This technique allows for probe-free measurement of forces, but has insufficient temporal resolution for the measurement of forces produced by many behaving animals, despite recent improvements (20). A second approach revolves around the use of micropillar arrays; in this technique, horizontally-aligned traction forces are measured by observing the deflection of pillars made of an elastic material with known mechanical properties. This approach can be limited in spatial resolution and introduces a non-physiological substrate that may influence animal behavior (21,22).

Recently we have introduced a technique named Elastic Resonator Interference Stress Microscopy (ERISM) which allows for the optical mapping of vertically aligned GRFs in the nanonewton range with micrometre precision by monitoring changes in local resonances of soft and deformable microcavities. This technique allows reference-free mapping of substrate interactions as well as calculation of vertically directed GRFs used in cell migration (23–25). Until recently, this technique was limited by its low temporal resolution (~10s) making it unsuitable for use in recording substrate interaction during fast animal movements, but a very recent further development of ERISM known as wavelength alternating resonance pressure microscopy (WARP),

has been demonstrated to achieve down to 10ms temporal resolution (26). Given ERISM and WARP allow for probe-free measurement of vertical ground reaction forces with high spatial and now temporal resolution, it becomes an attractive method for animal-scale mechanobiology.

In parallel, great strides have been made in understanding the neural and genetic underpinnings of locomotion in the *Drosophila* larva (27–31) a genetically tractable soft-bodied model organism (32). *Drosophila* larvae are segmentally organised peristaltic crawlers that move by generating waves of muscle contractions (3,31). Larvae have segmentally repeating bands comprised of 6 rows of actin trichomes (denticles) (33). The developmental and genetic origins of these structures have been extensively studied, but relatively little is known about how they are articulated during movement. While computational modelling and biomechanical measurements have provided an initial knowledgebase (34–36), data on biomechanical forces generated during substrate interactions in *Drosophila* larvae remain extremely limited (37,38). Development of methods for measuring GRFs in this model organism would enable fully integrated neurogenetic-biomechanical approaches to understanding soft-bodied movement and fulfil calls from the modelling community for more biomechanics data (39).

Here, we develop ERISM and WARP based approaches to measure GRFs exerted by freely behaving *Drosophila* larvae. We combine these measurements with kinematic tracking to explore how soft-bodied animals overcome fundamental biophysical challenges of moving over terrain. We find that, despite their legless appearance, *Drosophila* larvae interact with substrates by forming and articulating foot-like cuticular features ('protopodia') and cuticular papillae, which act as dynamic, travelling anchors. The use of ERISM-WARP provides a step-change in capability for understanding how soft-bodied animals interact with substrates and paves the way for a wider use of optical force measurement techniques in animal biomechanics and robotics research.

Results

Kinematic tracking of substrate interfacing features

As a first step in understanding how larvae interact with substrates, we confined 3rd instar larvae to glass pipettes lined with soft agarose (0.1% w/v) (**Figure 1A**). This allowed us to laterally image the animals and the lateral edges of denticle rows at the substrate interface (**Figure 1B**) while animals crawled towards an appetitive odour source. Animals interact with the substrate by large, soft, segmentally repeating cuticular features that contain rows of denticles and to which we refer as 'protopodia' in the following. Protopodia in each segment engaged in 'swing' periods (moving, SwP) and 'stance' periods (planted on substrate, StP) as waves propagated through the body. During SwPs, protopodia detached from the substrate, with the posterior row of denticles moving to meet the anterior row of denticles, thereby inverting the cuticle and sequestering the whole protopodia into a travelling pocket (**Figure 1C**). When protopodia ended their SwP, they unfolded from the sequestration pocket and then protruded into the substrate during the StP.

To further investigate the dynamics of protopodia placements, we performed detailed kinematic tracking of the morphometry of protopodia, denticle bands, and inter-protopodial spaces during peristaltic waves. By tracking the movement of defined points on bands relative to each other, we monitored intersegmental and intra-segmental movements during peristaltic waves (**Figure 2A**). In addition to moving relative to each other, denticle bands changed their shape during the sub-phases of a peristaltic wave. During forward waves (peristaltic contractions travelling in an anterograde direction), the anterior-most row of each denticle started to move after the corresponding posterior-most row (**Figure 2B**) and completed its movement after the posterior-most row stopped moving (**Figure 2C**), i.e. there was an anteroposterior (AP) latency for both Swing Initiation (SI) (when movement begins) and for Swing Termination (ST) (when movement ends). Such a 'rolling' progression pattern is analogous to the 'heel-to-toe' footfalls of limbed

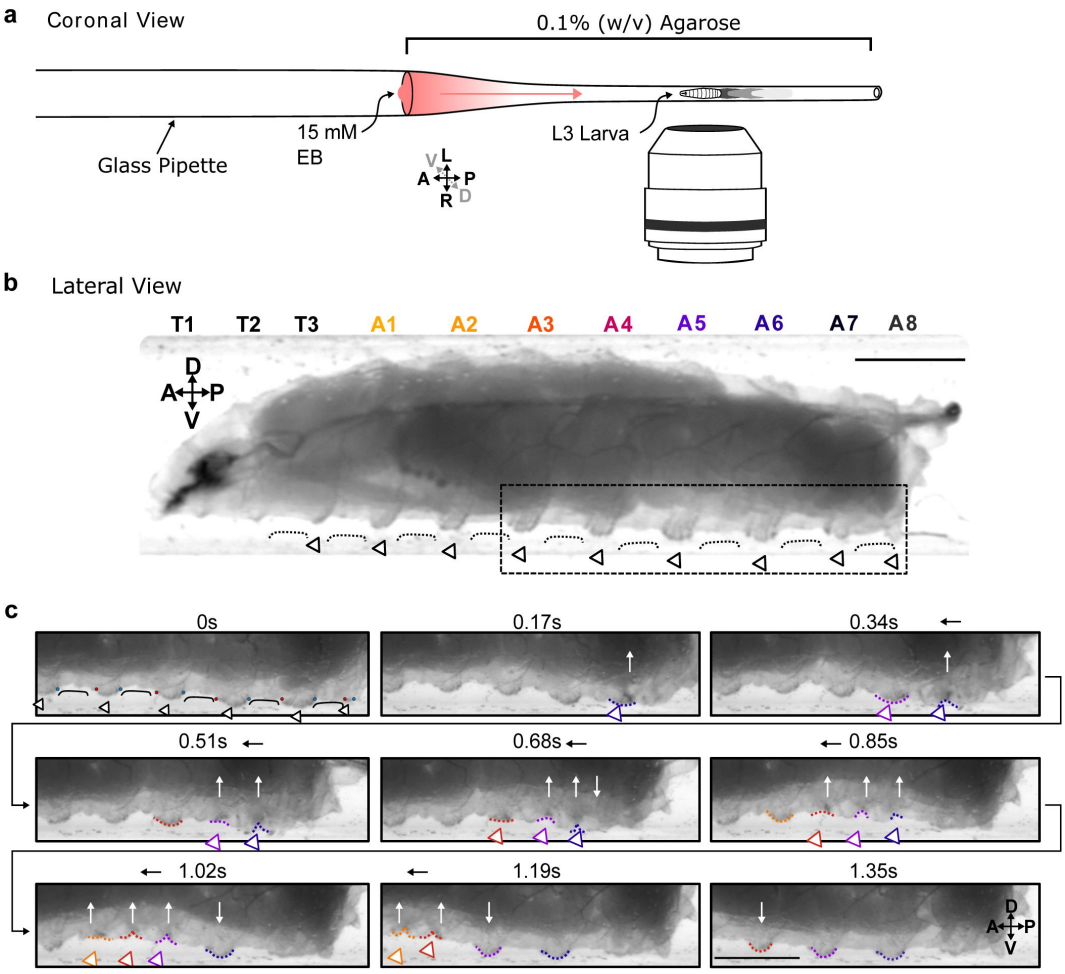

Figure 1.

Protopodia protrusions in each segment are sequestered during swing phases of forwards locomotion.

a, Schematic of setup for lateral imaging of larvae, using confinement in Pasteur pipette pre-filled with 0.1% (w/v) agarose. To encourage forward crawling, 10µl of 15mM ethyl butanoate (EB) was placed as attractive odour at the end of the pipette. **b**, Lateral brightfield image of 3rd instar larva showing convex areas of denticle bands (open arrowheads) protruding into the substrate, interdigitated by concave areas of naked cuticle (black line) not interacting with the substrate. Scale bar=750µm. **c**, Time lapse of area marked by dotted box in **b** showing the swing periods and stance periods of protopodia (coloured open arrowheads and dotted lines) during a forward wave. Red and blue dots at 0s denote anterior and posterior rows of denticles, respectively. As the posterior-most denticle row moved to meet the anterior row of the band, the medial row detached from the substrate via invagination (white arrows). The invaginated pocket is then moved forward (black arrow) and subsequently replanted. This action repeats as the wave propagates. Scale bar=500µm. Images representative of three 3rd instar larvae.

animals (40). To analyse this pattern further, we quantified the percentage of the wave duration spent in AP latency during SI and ST. For forwards waves, this relative latency was generally consistent across the denticle bands on large protrusive protopodia but less pronounced for the smaller and less protruding protopodia at the extreme posterior and anterior abdomen and the thorax (**Figure 2D**). In backwards waves, the heel-toe like latency was reversed, with anterior-led latencies observed in SI and posterior-led latencies observed in ST (**Supplementary Figure S1**).

In summary, each segment-wise denticle action event is composed of four distinct periods: SI, SwP, ST, and StP. For forward waves and posterior segments, the latencies during the SI period are largely determined by wave duration (R^2 range: 0.46-0.78, A7-A4) but this is less the case for anterior abdomen and thorax (R^2 range: 0.12-0.35, A3-A1 and T3, **Figure 2E**). The magnitudes of ST-related latencies are not strongly strongly determined by wave duration (R^2 range: 0.01-0.26, **Figure 2F**).

Developing stress microscopy for *Drosophila*

Kinematic analysis of protopodia movements revealed a previously uncharacterised complexity in the dynamics of larval movement, but it cannot quantify the mechanical forces impacting the substrate and is therefore limited to making inferences regarding substrate interaction. To achieve quantitative observations, we therefore adapted ERISM-WARP (**Figure 3A**, **Supplementary Figure S2**) to map the vertically directed GRFs exerted by larvae rather than the forces exerted by single cells. First, we developed optical microcavities with mechanical stiffnesses in the range found in hydrogel substrates commonly used for studying *Drosophila* larval behaviour, i.e. Young's modulus (E) of 10-30kPa (41–43). These microcavities consisted of two semi-transparent, flexible gold mirrors sandwiching a transparent polymer rubber that was made from a mixture of siloxanes with discrete Young's moduli to adjust the resulting stiffness (44). The microcavities were characterised using atomic force microscopy (AFM) and the resulting force distance curves (**Figure 3B**) were fitted to a height-corrected Hertz Model to determine the Young's modulus of each cavity (45). This procedure allowed us to fabricate microcavities with a wide range of well-defined Young's moduli (**Figure 3C**, **Supplementary Table 1**).

As an initial test, we placed cold-anaesthetised 2nd instar larvae onto a microcavity (E=28kPa) and performed ERISM force mapping at different magnifications to record substrate indentations generated by larval body features (**Figure 3D-L**). Indentation maps were computed from the images of optical interference by pixelwise solving of the resonance condition with an optical model. Stress maps were then computed from the indentation maps via a finite element method (FEM) simulation of the stress distribution required to produce the observed indentation profile (Methods; the accuracy of our calculations was confirmed applying a known force with an AFM, **Supplementary Figure S5**). With this approach, we were able to resolve indentations from rows of denticle bands interdigitated by naked cuticle (**Figure 3G-I**). At higher magnification and when using slightly softer microcavities (E=19kPa), even indentations from individual denticles within these bands were resolved (**Figure 3J-L**). The median force exerted by individual denticles was 11.51nN (1.4nN-47.5nN; n=130 denticles) across a median area of 2.81µm (1.15-9.13µm; n=130 denticles).

Videorate force mapping in freely behaving animals

Next, we moved to force mapping of freely behaving animals. First, we confirmed that ordinary larval behaviour is maintained on collagen-treated microcavity substrates (**Supplementary Figure S3**). We then adapted WARP (26) to image substrate interactions at high temporal resolution (**Supplementary Figure S4**). For forward peristaltic waves, we observed posterior to anterior progressions of indentations into the cavity, corresponding to protopodial placements (**Figure 4A**). We also observed upward deflections of the substrate (i.e., increase in microcavity thickness, positive stress), associated with the displacement of elastomer because of Poisson's ratio

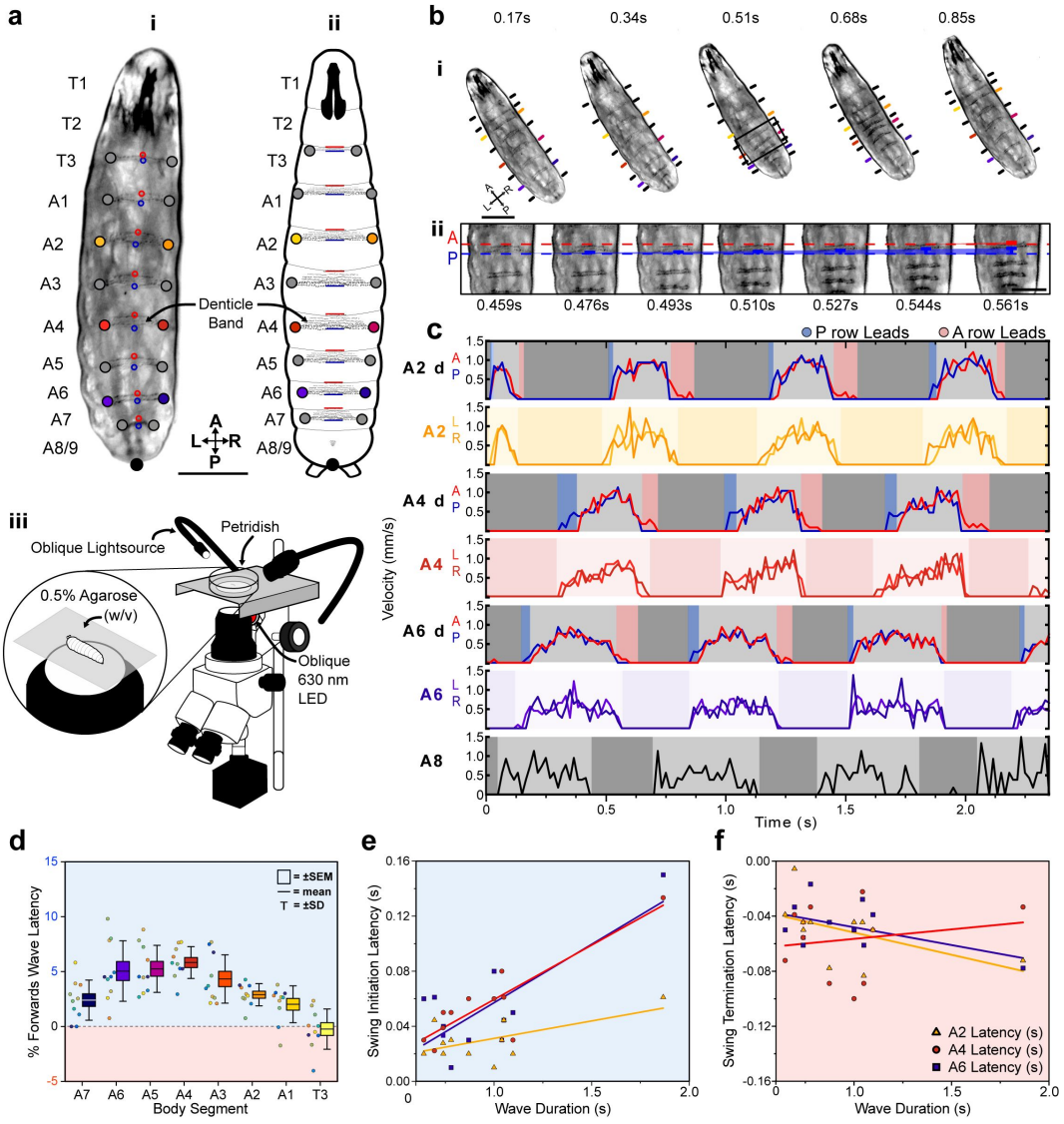

Figure 2.

Protopodia kinematics follow ‘heel-toe’-like footfall dynamics.

a, (**i**) Brightfield image and (**ii**) schematic of 2nd instar larvae showing ventral side denticle belts which reside upon the protopodia and (**iii**) schematic of the imaging setup used for kinematic tracking. Scale bar=200μm. **b**, (**i**) As a forward wave travels through the animal, the distance between denticle bands decreases. Scale bar=200μm. (**ii**) At higher frame rate and magnification, changes in distance between the posterior and anterior most denticle rows are resolved. The posterior-most row (P, blue) initiates movement first and moves until nearly reaching the anterior-most row (A, red) at 0.544s, after which point, they move together (0.561s). Scale bar=100μm. **c**, Velocity of anterior- and posterior-most denticles rows (A2d A/P, A4d A/P, A6d A/P) and the left/right end of denticle bands (A2 L/R, A4 L/R, A6 L/R and A8 L/R) over three representative forward waves, showing how the strategy observed in **b** is maintained across body segments. Background colours indicate swing initiation (SI, blue), swing period (SwP, light grey), swing termination (ST, pink) and stance period (StP, dark grey). **d**, Forward wave latency for different animals and body segments. Positive values denote posterior row led latency. n=10 animals, 30 waves. **e**, SI-latency scales with wave duration in the posterior abdomen (A6: R^2=0.61, purple; A4: R^2=0.78, red) but less so for the anterior abdomen (A2: R^2=0.35, yellow). n=12 animals with 3 latency periods per segment. **f**, ST-latencies do not scale with wave duration (A6: R^2=0.26, A4: R^2=0.26, A2: R^2=0.03). n=12 animals with 3 latency periods per segment.

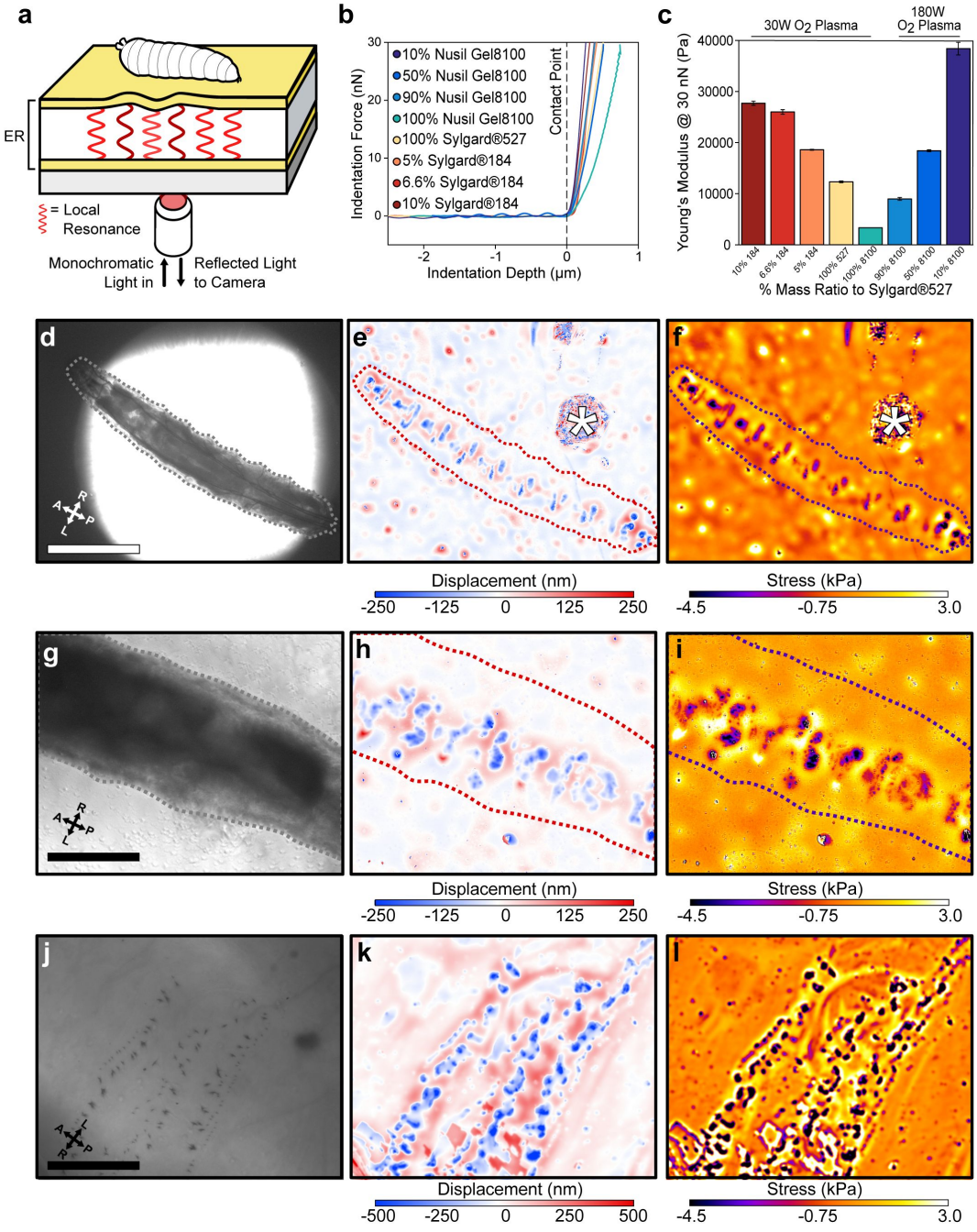

Figure 3.

ERISM maps mechanical substrate interactions in *Drosophila* larvae.

a, Schematic of setup for ERISM with *Drosophila* larva on an optical microcavity. Maps of local cavity deformation (displacement) due to indentation forces are generated by analysing cavity resonances. **b**, Force distance relationship measured by AFM and **c**, Mechanical stiffnesses (Young's moduli) for microcavities produced by mixing different elastomers at different ratios and applying different plasma conditions. **d**, **g**, **j**, Brightfield images of anaesthetised 2nd instar larvae recorded at low, medium, and high magnification. **e**, **h**, **k**, Corresponding maps of microcavity displacement. (* denotes contamination on cavity surface from handling the larva.) **f**, **i**, **l**, Corresponding maps of mechanical stress obtained by finite element analysis of displacement maps, showing the stress on the substrate due to passive interaction between larvae and substrate. Scale bar=500μm (**d**), 250μm (**g**) and 50μm (**j**). Images representative of 4 separate 2nd instar larvae. Microcavities in **d**-**i** used 30W O_2 10% Sylgard®184 design, and **j**-**l** used a 30W O_2 5% Sylgard®184 design.

governing elastic materials (46). We also observed that the animals travel surrounded by a relatively large water droplet. During StP, protopodia displaced the substrate, and during SwP, protopodia local to the contraction were completely removed from the substrate while travelling to their new resting position.

We also used WARP to investigate the bilaterally asymmetric head sweeps generated by *Drosophila* larvae to sample odours and direct navigation. During head sweeps, anterior segments and mouthhooks detached or dragged across the substrate before replanting (**Figure 4B**). 0.5-1s prior to headsweep initiation, the contact area in posterior segments increased, spreading outwards laterally, employing both the protopodia and the naked cuticle along the midline (**Figure 4C**). This broad but shallow anchoring quickly returned to the ordinary resting phase profile after the mouth hooks were replanted onto the substrate (**Figure 4D**).

Before forwards waves and headsweeps, larvae produced large indentations posterior to their terminal segment. Anatomical examination revealed accessory structures located at the terminus of the posterior abdomen. Together with the terminal denticle band, these cuticular processes generated tripod-shaped indentation patterns (**Figure 4E**). The left and right sides of the tripod deployed and detached simultaneously (**Figure 4F**). Tripod formation was seen before all observed forwards waves (n=28 across 6 animals) and bilateral thoracic activity (n=3 across 2 animals), but not all tripod contacts resulted in further behaviour (**Figure 4G**). To investigate the relationship between tripod placement and locomotion further, we recorded the delay between tripod contact and protopodial detachment in A7. The mean delay was 0.66s±0.21s (**Figure 4H**, n=20 waves across 6 animals).

Next, to estimate the GRF associated with the indentation of each protopodium, we integrated the displacement and stress maps over the region covered by each protopodium. During forward waves, the temporal evolution of GRFs mirrored the characteristics of the cycle seen in the stress maps, with absolute GRFs ranging between 1 and 7μN (**Figure 5A**). However, unexpectedly, we observed an additional force applied to the substrate both when protopodia leave the substrate (SI) and when they are replanted (ST). To investigate whether this force was due to an active behaviour or due to shifting body mass, we plotted protopodial GRFs against the contact area for each protopodium over time, combining data from multiple forwards waves (**Figure 5B**). We found that the magnitude of force output was positively correlated with protopodial contact area in a quadratic relationship (A6: Adj. R^2=0.77, A4: Adj. R^2=0.92, A2: Adj. R^2=0.79) Comparing different animals, we find that GRFs were relatively consistent across most segments (**Figure 5C**).

The contact area of each protopodium showed a pronounced peak during SI and ST. The maximum contact area during ST was significantly greater than during SI for the posterior abdomen ($p \leq 0.05$ for A8/9-A3) but not for the anterior abdominal protopodium ($p > 0.05$ for A2) (**Figure 5D**). The peak of the displaced volumes during SI was largely determined by wave duration (R^2 range: 0.48-0.69, A7-A4, **Figure 5E**), again except for the anterior abdomen (A3: R^2=0.15; A2: R^2=0.24). However, the peak of the displaced volumes during ST did not scale with wave duration (R^2 range: 0.03-0.05, A7-A2). This suggests that protopodia push off from the substrate harder during faster waves, but that varying wave speed does not strongly influence forces exterted onto the substrate during protopodia placement. This observation is consistent with our morphometric data, which showed that wave duration is associated with SI latencies but not with ST latencies.

Sub-protopodial force dynamics

Lastly, to investigate how forces are translated into the substrate within a single protopodium during a 'footfall' cycle, we examined the spatiotemporal substrate interaction during the ST (**Figure 6A**). This showed how protopodia expand their indentive contact across both the AP and mediolateral (ML) axes when being replanted. Kymographs along the AP midline of animals and profiles running up the AP axis extracted from these revealed a delay between when the most

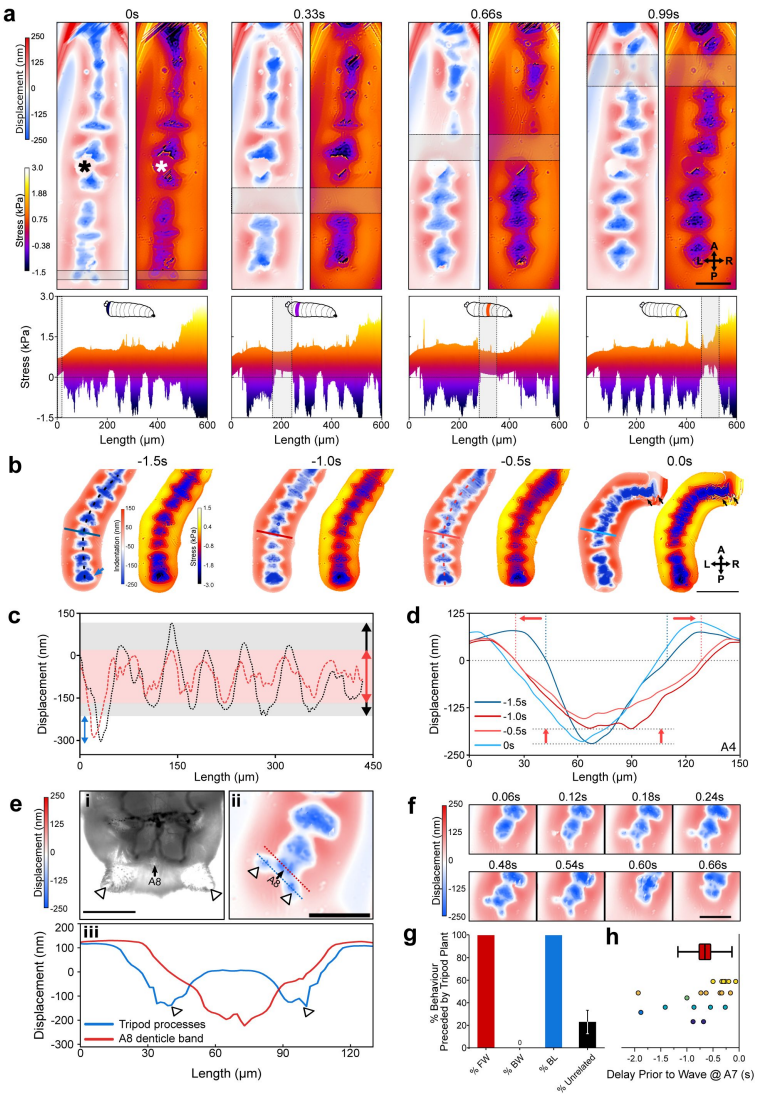

Figure 4.

WARP imaging reveals dynamics of substrate interactions during larval movement.

a, WARP image sequence of displacement and stress maps (top) for a freely behaving 2nd instar larva during forward locomotion. (*denotes dust artefact.) Lateral projections of stress maps (bottom) showing individual protopodia interdigitated by naked cuticle. As a contractile wave (grey box) progressed through the animal, protopodia were lifted off the substrate. Scale bar=100μm. **b**, WARP image sequence of larva prior to (-1.5s to -0.5s) and engaging in (0s) a headsweep (representative of 2 animals and 3 turns). Note the large posterior displacement (blue arrow)(Images cropped around the animal). Scale bar=200μm. **c**, Profiles of cavity displacement along anteroposterior (A-P) axis in resting state (black dotted line at -1.5s in **b**) and pre-headsweep (red dotted line at -0.5s in **b**), showing that peak displacement decreased across all segments from the resting state (grey box) to pre-headsweep (pink box). **d**, Bilateral displacement profile across the mediolateral (ML) axis of the A4 protopodium (solid lines in **b**) at different times prior to the headsweep, showing that the width of the contact increases from the resting state (- 1.5s) to the pre-headsweep state (-0.5s) and partially reduces again immediately after head movement. **e**, (**i**) Brightfield image (3rd instar larva) and (**ii**) displacement map (2nd instar larva) of the posterior-most body segment, showing how two cuticular protrusions (white arrowheads) and the terminal protopodium (A8) generate a tripod-shaped substrate displacement. (**iii**) Profiles along blue and red dotted lines in (ii). Scale bar=200μm (i) and 100μm (ii). **f**, Sequence of displacement maps of tripod structure before the start of a forward wave (<0.24s) and the removal of tripods upon beginning of peristalsis (>0.48s). Scale bar=100μm. **g**, Percentage of forward waves (FW), bilateralisms (BL), backward waves (BW) preceded by tripod contact, and tripod deployments without any observed locomotor behaviour (unrelated). **h**, Time delay between tripod deployment and initiation of movement at A7. Points colour-coded by animal, n=6. Line=mean, box=±1 standard error of the mean, whiskers=±1 standard deviation.

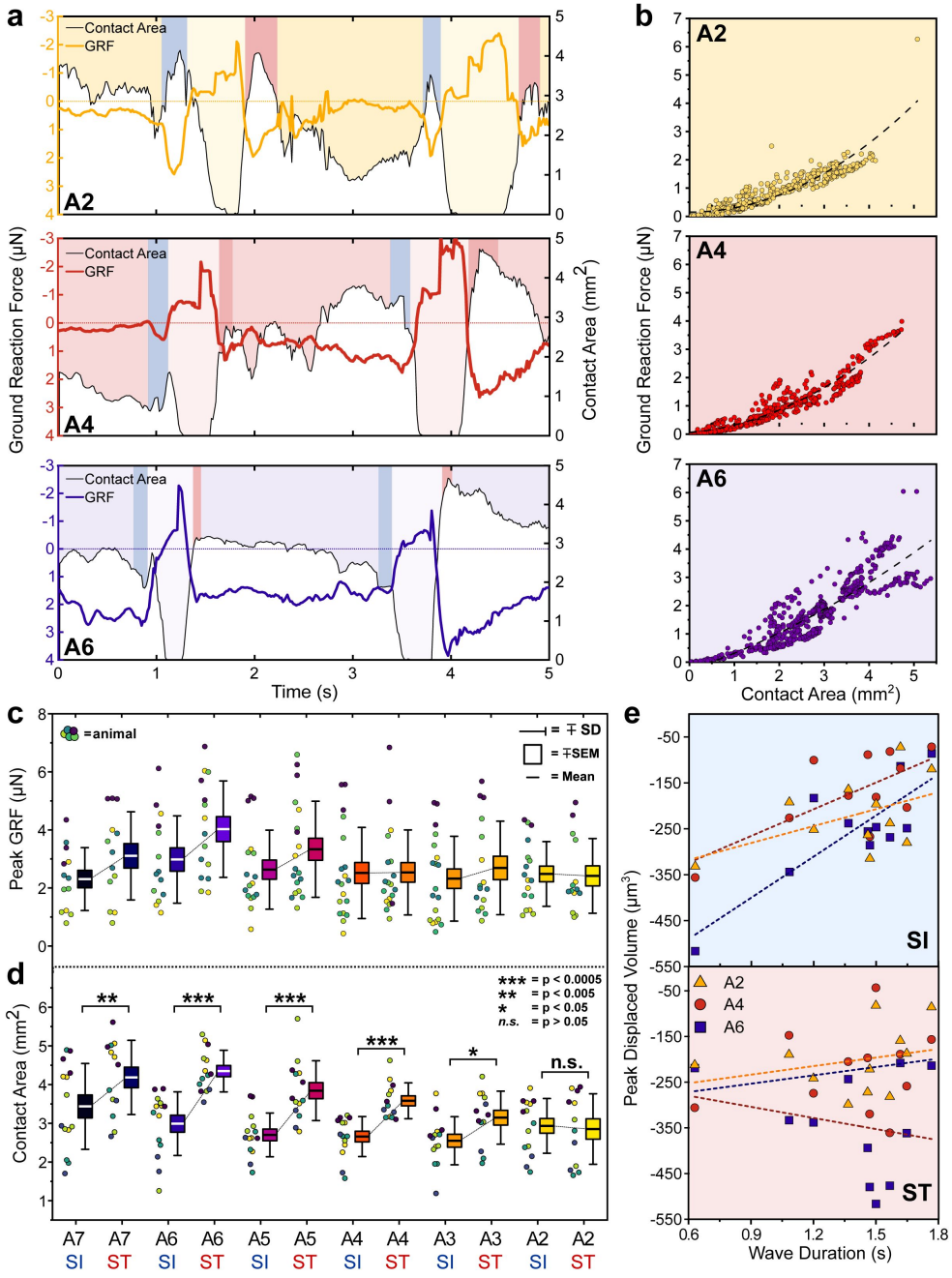

Figure 5.

Protopodia produce GRFs in the micronewton range and show complex spatiotemporal dynamics.

a, Ground reaction force (GRF, coloured line) and protopodial contact areas (white area under black line) during forward crawling for A2, A4 and A6 protopodia, showing progression of waves through animal (light-coloured boxes). Blue (SI) and pink (ST) boxes denote characteristic troughs in GRF immediately prior to protopodia leaving the substrate and returning to the substrate, respectively. **b**, GRFs exerted by different protopodia show a 2nd order polynomial relationship (dashed line) with the contact area of that protopodium (A6: Adj. R^2=0.77, A4: Adj. R^2=0.92, A2: Adj. R^2=0.79). Peak GRFs and **d**, peak contact area during SI and ST across body segments. Data points denote single events, colours indicate different animals. n=5, 15 waves. Contact areas were compared by a two-way repeated measures ANOVA (*<0.05, **<0.005, ***<0.0005, n.s.=not significant). **e**, During SI, peak displaced volume scaled with wave duration for larger abdominal segments (A6: R^2=0.69; A4: R^2=0.48) but not for smaller anterior segments (A2: R^2=0.24). During ST, displaced volume did not scale with wave duration regardless of the segment (A6: R^2=0.05; A4: R^2=0.05; A2: R^2=0.08). n=4, 11 waves.

posterior and the most anterior part of the protopodium contacts the substrate (**Figure 6B**). The mean contact delay relative to the most posterior part of the protopodium was 0.035s±0.007s at 6μm away from the most posterior part and increased to 0.062s±0.021s and 0.253±0.115s in the middle and at the most anterior part of the protopodium, respectively (**Figure 6C**).

To examine how protopodia expand along the ML axis, we performed a similar analysis, taking kymographs and profiles for the displacement maps at different distances to the midline of a protopodium. At a medial distance from the midline, the contact delay relative to the midline was 0.045s±0.022s (left) and 0.057s±0.019s (right). At the distal left and right of the protopodium, contact occurred 0.111s±0.030s (left) and 0.165s±0.058s (right) after midline contact (**Figure 6D**). This analysis also showed that protopodia insert a medial-spike into the substrate, through which ST related peak GRFs are conferred, before expanding along the AP and ML axes.

Discussion

Drosophila larvae, though legless, have protopodia

The cuticle of larvae shows distinct patterns of denticulation (denticle bands) and the developmental processes which give rise to these features have been well studied (33) though their role in locomotion has long been unclear (47). Here, we show that denticle bands are situated upon larger articulated foot-like cuticular processes, which act as locomotory appendages. Protopodia dynamically change shape during locomotion, allowing sequestration and presentation of denticles. Individual protopodia and individual denticles exert GRFs in the 1-7μN and 1-48nN ranges, respectively. Superficially, protopodia resemble the much smaller pseudopodia in cells – transient structures, similarly covered with actin protrusions, used by cells to facilitate movement (48). The same function and principles of protopodia may underlie 'creeping welts' noted in larger dipteran larvae (49) and show similarities to soft prolegs of *Manduca sexta* caterpillars but are approximately 30 times smaller (8).

Insights from morphometric kinematic tracking of denticle band movements

Our study provides, to our knowledge, the first detailed description of the morphometry of denticle bands during movement, showing how denticle bands are deployed onto and removed from the substrate. Posterior denticle rows hit the substrate before anterior rows during deployment (ST) and left the substrate before anterior rows during removal (SI). This suggests that both deployment and removal involved rolling 'heal-toe' like movements, similar to footfalls in limbed animals, including terrestrial arthropods (40). Removal but not deployment correlated with wave duration. In *Manduca* caterpillars, it has been noted that SwPs scale positively with wave duration (50); however, to our knowledge there is no measurement for SI and ST in these animals.

SI latencies scaled positively with wave duration across most segments whereas ST latencies did not show this trend. SIs scale with SwP and this could be mediated by proprioceptor activity in the periphery (51). Fine sensorimotor control of musculature during this process would allow for precisely tuned propulsion during peristalsis. In contrast, the more random nature of the ST suggests the process is less finely controlled. This could be a consequence of fluid inertia within the animal, and/or the release of elastic energy from cuticle (38) or relaxation of muscles (50,52).

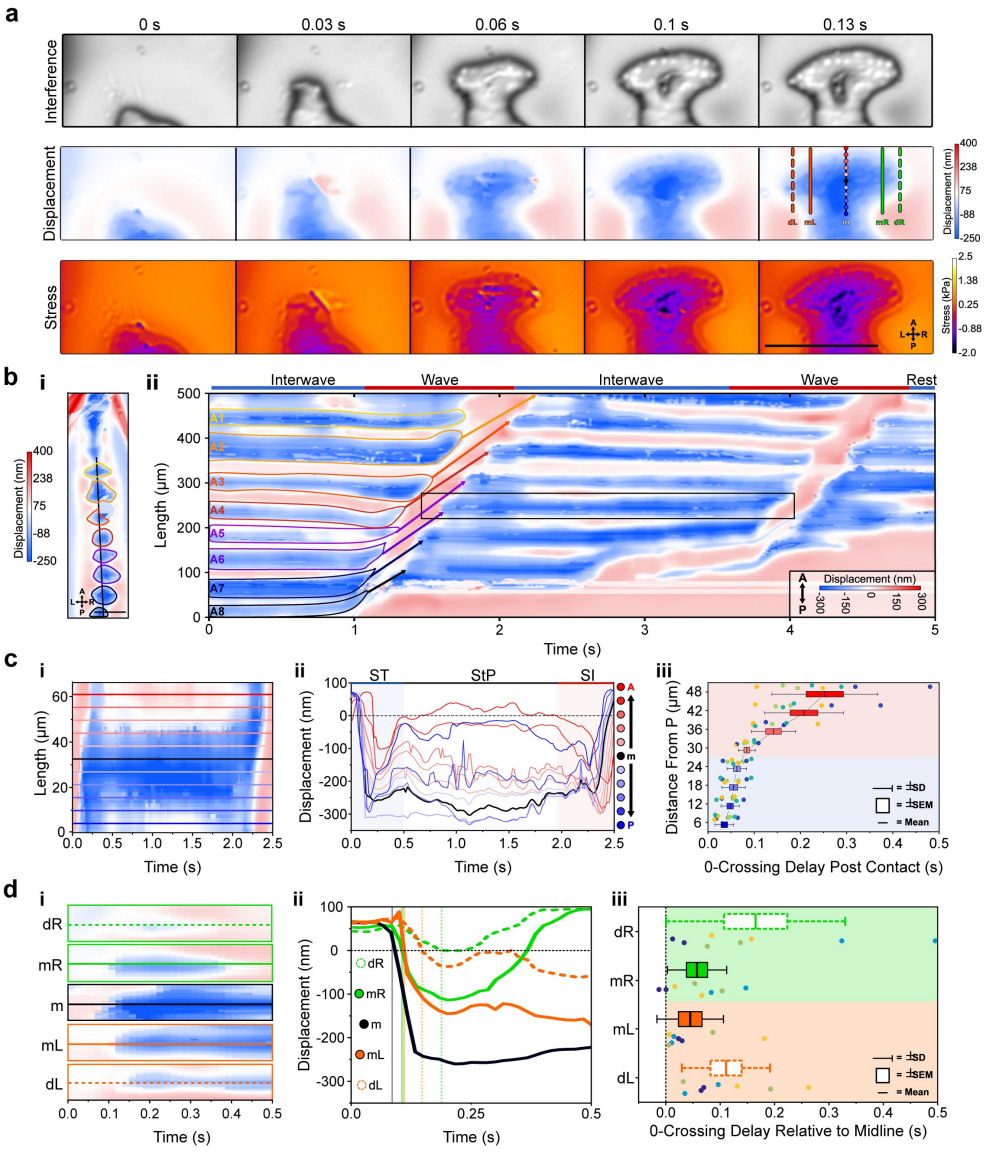

Figure 6.

Sub-protopodial force dynamics reveal sub-step processes and functional substrate interfacing domains in each step.

a, WARP imaging of protopodial landing during ST of an A6 protopodium. Raw interference images from WARP acquisition show footprints of individual denticles as white dots. Displacement and stress maps show how landing starts with posterior denticle rows before spreading out along the AP and ML axes. Scale bar=100µm. **b**, **(i)** Displacement map of whole animal. **(ii)** Kymograph of displacement along AP axis (black line in i) over 2 forward waves. Bands of red and blue correspond to naked cuticle and protopodia, respectively. Scale bar=100µm. **c**, (**i**) Kymograph of displacement along the AP axis of an A6 protopodium (box in **b**). (**ii**) Profiles across kymograph at different positions along the AP axis of protopodium (lines in i). (**iii**) Latency of substrate indentation (displacement <0nm) during ST along the AP axis, relative to the extreme posterior of protopodium. Compared to the posterior half of protopodium (light blue area), the anterior half shows larger latencies and variations in latency (light red area). n=4 animals, 8 swing termination events. **d**, Kymograph of displacement along AP axis during ST for the distal left (dL), medial left (mL), midline (m), medial right (mR) and distal right (dR) section of the A6 protopodium. Height of each kymograph, 66.42µm, (**ii**) Profiles across the central AP line of each kymograph in (i). Vertical lines indicate times when midline, medial right/left and distal right/left indentation starts (displacement <0nm). (**iii**) Latency of substrate indentation during ST relative to the midline for medial right/left and distal right/left locations. n=4, 8 swing termination events.

ERISM-WARP allows computation of ground reaction forces in *Drosophila* larvae

We adapted state-of-the-art mechanobiological force measuring techniques to enable measurement of substrate interaction dynamics of a freely behaving soft-bodied animal with micrometer spatial resolution, millisecond temporal resolution and nanonewton force resolution. Previously, high-resolution force mapping was limited to cellular mechanobiology. Specifically, we developed microcavity resonators tuned to the vertical forces generated by larvae and employed ERISM and WARP to perform direct measurements of substrate interactions in anesthetized and behaving animals. GRFs produced by individual denticles in anaesthetised animals were in the ~11nN range. The measured vertical GRFs produced by the individual protopodia of each segment were in the 1 to 7μN range, roughly three orders of magnitude less than the 17mN recorded from an entire 1.72g *Manduca sexta* caterpillar (8). Our measurements provide fundamental constraints for future biomechanical modelling studies seeking to incorporating these structures.

Displacement and stress maps produced during larval crawling revealed that animals can control when and how protopodia contact the substrate. We observed that larvae travel surrounded by moisture from a water droplet, which produces a relatively large upwardly directed force in a ring around the animal. This surface tension produced by such a water droplet likely serves a role in adhering the animal to the substrate. However, during forward waves, we found that protopodia detached completely during SwP, suggesting this surface tension-related adhesion force can be easily overcome by the behaving animal. This observation, coupled with our lateral imaging of protopodia in constrained animals, explains how larvae prevent their rough denticulated cuticle from creating drag due to friction against the direction of the wave. Larvae do not simply pull protopodia off the substrate in a vertical direction; instead, they horizontally slide posterior regions forward in the axis of travel, before invaginating and therefore sequestering friction generating features (e.g. denticles). This shows similarities to the use of shearing forces to detach adhesive pads in limbed arthropods (40) Inversion of the cuticle to remove denticles from the substrate may also explain why natural variations in denticle count across animals do not strongly affect locomotor behaviour (47). The invagination process is reversed in order to expand the protopodia into and locally across the substrate, providing an expanding anchor which can serve as a postural support to enable locomotion and prevent lateral rolling during bilaterally asymmetric behaviours such as head sweeps. The dynamic anchoring during the progression of peristaltic waves thus serves to counteract horizontal reaction forces resulting from Newton's 3rd law of motion. Such a sequence of positioning points of support and anchoring them against the substrate has long been postulated to be a fundamental process in soft-bodied locomotor systems (6); and may be central to explaining why soft-bodied animals have evolved segmentally repeating bodies (53). However, WARP microscopy is largely limited to measurements of forces in the vertical direction, and though we can make inferences such as this as they are a consequence of fundamental laws of physics, we present this conclusion as a testable prediction which could be confirmed using a force measurement technique more tuned to horizontally directed forces relative to the substrate.

Our ERISM-WARP measurements also revealed substrate interaction from accessory structures. Immediately before enacting headsweep, larvae redistributed their body mass into naked cuticle in between protopodia along the midline, effectively fusing multiple protopodia into a single 'ultra-protopodia' that extends across multiple posterior segments. This redistribution occurs hundreds of milliseconds before the start of a head sweep, suggesting that it may be part of an active preparatory behaviour. Similar preparatory behaviours have been observed in caterpillars before cantilevering behaviours (10), adult flies during fast escape behaviours (54) and humans during stepping (55). More detailed characterisation of this behaviour remains a challenge owing to the changing position of the mouth hooks. Due to their rigid structure and the

relatively large forces produced in planting, mouth hooks produce substrate interaction patterns which our technique struggles to map accurately due to overlapping interference fringes ambiguating the fringe transitions.

We also observed transient tripod-shaped substrate interactions in posterior terminal regions of larvae immediately before forward waves and headsweeps. Two bilateral cuticular protrusions covered in trichomes, labelled in previous work as anal papillae (56), are likely candidates responsible for these substrate interactions. However, the actions of these structures have hitherto not previously been described as a part of movement in soft-bodied animals. Each body segment has a preceding substrate-planted segment which acts as the anchor and lever to push the animal forward. However, A8 is an exception; it has no full preceding segment in contact with the substrate to counteract its muscle contraction. The tripod processes are ideally positioned to provide an anchor against horizontal reaction force generated by by the initial contraction when moving forward (**Figure 7A**), and might effectively form a temporary extra segment prior to initiation of a wave (**Figure 7B**). The deployment of cuticular features as transient anchors has not been a focus of previous studies; future work should incorporate our findings into models of crawling behaviour. WARP and ERISM have technical limitations, such as the difficulty of resonator fabrication. This problem is compounded by the fragility of the devices owing to the fragility of the thin gold top mirror. This becomes problematic when placing animals onto the microcavities, as often the area local to the initial placement of the animal is damaged by the paintbrush used to move the animals. Further, as a result of the combining of the two wavelengths, the effective framerate of the resultant displacement and stress maps is equal to half of the recorded framerate of the interference maps. This necessitates recording at very high framerates and thus requires imaging at reduced image size to maximise framerates, but this in turn reduces the number of peristaltic waves recorded before the animal escapes the field of view. A further limitation is that WARP and ERISM are sensitive mainly to forces in the vertical direction; this is complementary to TFM, which is sensitive to forces in horizontal directions. Using WARP in conjunction with high speed TFM (possibly using tuneable elastomers presented here) could provide a fully integrated picture of underlying vertical and horizontal traction forces during larval locomotion.

Evidence for functional subdivisions within protopodia

By examining the dynamics of individual footfalls, we found that protopodia exhibited characteristic spatiotemporal force patterns across the footfall cycle. This shows parallels to the regional specificity of function in a vertebrate foot. Specifically, the posterior medial region of the protopodia makes a large contribution to peak GRFs exerted during ST (**Figure 7B**), similar in nature to a vertebrate heel strike impacting the surface prior to the rest of the foot. We propose that this zone of the protopodia acts as a vaulting point for the protopodia, functioning as a 'point d'appui' (point of support) as proposed in other soft-bodied animals (6,57). The transience of this vaulting point suggests it may be critical for locomotion, but dispensable for postural control during StP. The distal area of protopodia exhibited a similar transience. This increased force transmitted into the substrate is unexpected as the forces generated for the initiation of movement should arise from the contraction of the somatic muscles. We propose that the contraction of the musculature responsible for sequestration acts to move haemolymph into the protopodia thus exerting an increased pressure onto the substrate while the contact area decreases as a consequence of the initiation of sequestration. Immediately after the posterior and medial protopodia impact during ST, the contact area of the outer region of the protopodia grew across both the AP and the ML axes. However, throughout the StP, this outer region then slowly retracted, suggesting it too was not critically important for maintaining posture during StP. This may reflect a transient anchoring mechanism – specifically, this anchor region deploys to provide greater friction for the subsequent segments (**Figure 7C**). This would allow the contractile wave to progress unimpeded by resultant reaction forces. Previously, such a function was thought to be provided mainly by mucoid adhesion (6). However, *Drosophila* larvae are proficient at crawling

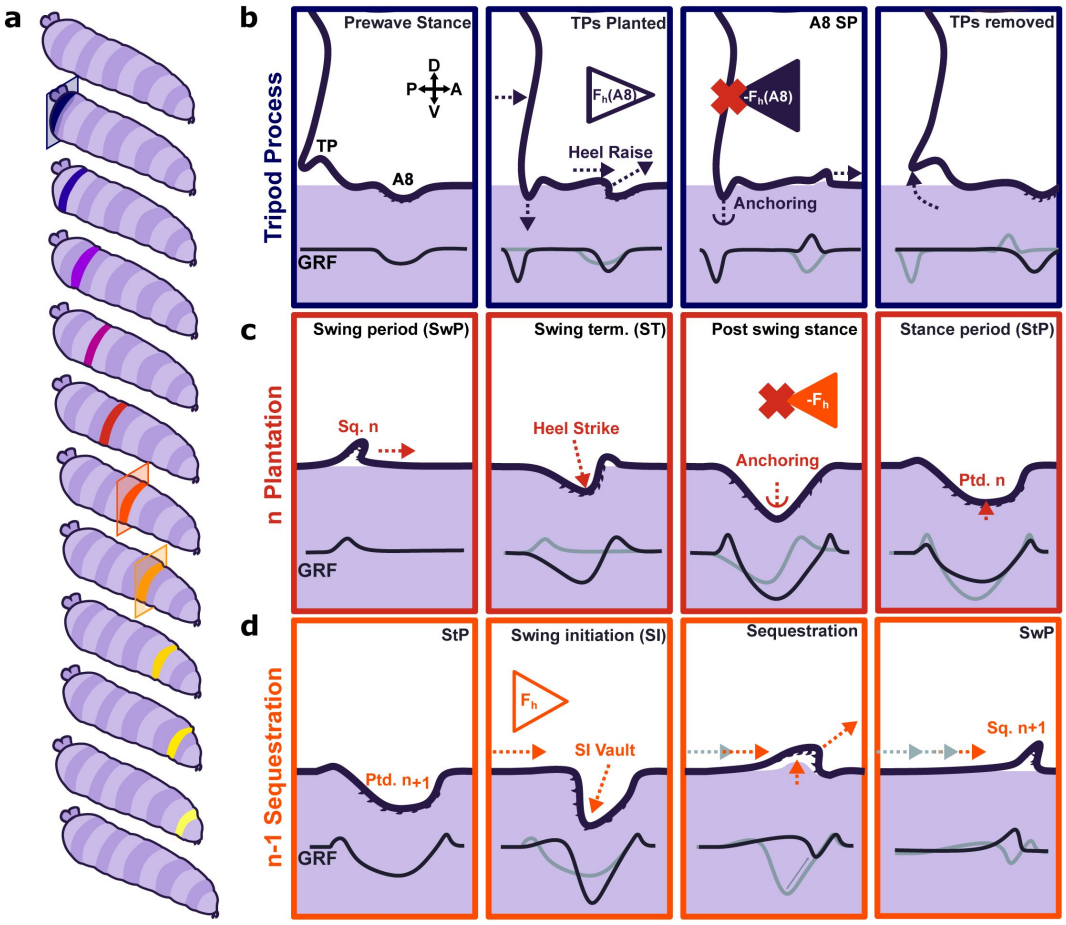

Figure 7.

Proposed model for protopodia-substrate interactions during *Drosophila* larval locomotion.

a, Schematic illustration of forward wave propagating from posterior (blue) to anterior (yellow). **b**, At the start of a forward wave, animals contract the posterior-most abdominal segment (A8), producing an anterograde horizontal force F_h(A8). Due to Newton's 3rd law, there is an equal but opposite reaction force -F_h(A8). To counteract this force, tripod processes (TPs) deploy onto the substrate and generate a temporary anchor, allowing the A8 protopodium to swing forward. **c**, During swing termination (ST) at the end of the swing period (SwP) of segment *n*, the corresponding sequestered protopodium (Sq. *n*) strikes the substrate with its posterior most denticle row, then gradually unfolds into the substrate along its entire anteroposterior extent. During the stance period (StP), this planted segment *n* (Ptd. *n*) forms an anchor to mitigate the retrograde reaction force due to the subsequent contraction of segment *n*-1. **d**, In time with anchoring of protopodium *n*, protopodium *n*-1 performs swing initiation (SI) by removing denticles from the substrate and sequestering into an invagination pocket, which reduces friction during the subsequent SwP. The contraction of segment *n*-1 then leads to an anterograde force (F_h) that is balanced by the anchoring of protopodium *n* as illustrated in **c**.

over wet surfaces where mucoid adhesion is reduced or impossible (43). Larvae can adhere to dry surfaces but have difficulty moving over these, although mucoid adhesion would provide optimal anchorage in this context. Water surface films appear to facilitate larval locomotion in general, but the biomechanical mechanisms by which this occurs remain unclear. We propose that protopodia act to provide an optimal balance between anchorage and adhesion depending on the environmental context. Overall, our work suggests that *Drosophila* larvae use a sophisticated process of articulating, positioning and sequestering protopodia to enable movement over terrain. Future work will be needed to determine the extent to which these processes are conserved across other soft-bodied crawlers.

Conclusions and outlook for future work

Combining ERISM-WARP with a genetically tractable model organism opens new avenues for understanding the biomechanical basis of animal behaviour, as well as the operation of miniaturized machines. Here we have provided new insights into the relatively well-studied behaviour of *Drosophila* larval locomotion. We have provided new quantitative details regarding the GRFs produced by locomoting larvae with high spatiotemporal resolution. This mapping allowed the first detailed observations of how these animals mitigate friction at the substrate interface and thus provide new insights into how locomotion is achieved in soft animals. Further, we have ascribed new locomotor function to appendages not previously implicated in locomotion in the form of tripod papillae, providing a new working hypothesis for how these animals initiate movement. It is our hope that these new principles underlying locomotion outlined here serve as useful biomechanical constraints as called for by the wider modelling community (39) We used *Drosophila* larvae as a test case, but our methods now allow elastic optical resonators to be tuned to a wide range of animal sizes and thus create new possibilities for studying principles of neuro-biomechanics across an array of animals. In parallel, roboticists are increasingly moving to create miniaturized soft robots for a variety of applications. Our approach is well suited to provide ground truth, constraints, and inspiration for the development of such miniaturized machines. It also provides a potentially powerful new resource for evaluating the performance of these devices, as our methodology will also allow scientists to measure GRFs during the operation of miniaturized soft machines. Importantly, while we have focused here on the movement of soft animals, our sensors could also be tuned to measure forces produced by small limbed animals or miniaturized machines with rigid internal or external skeletons. Overall, this work therefore establishes a flexible platform for future investigations aimed at integrating knowledge across genetics, neuroethology, biomechanics, and robotics.

Materials and Methods

Key Resources

Reagent type (species) or resource	Designation	Source or reference	Identifiers	Additional information
Animal (*Drosophila melanogaster*)	Canton S (wildtype)		FBsn0000274	
Software	OriginPro 2019b	OriginLab Corp		Statistical analysis and plotting
Software	COMSOL Multiphysics	COMSOL Inc.		Finite Element Method simulation resolving stress maps.
Software	Python 3.0 & 2.0	Anaconda Inc.		Cavity length map computation
Software	Inkscape v.1.01	Inkscape Organisation		Vector figure making

Software	FIJI	National Institutes of Health / SciJava	1.52p	Image Analysis and manual tracking
Chemical	Phosphate buffered saline			Collagen coating
Chemical	Hydrochloric acid 5M			Collagen coating
Chemical	Acetic acid 95%			Collagen coating
Chemical	Collagen-I	Millipore	L7220	Collagen coating
Fabrication material	Gold grains (99.99%)	Kurt J. Lesker Company	EVMAU40SHOT	Microcavity fabrication
Fabrication material	Chromium 99.95%	Kurt J. Lesker Company	EVMCR35 EJTCRXX351	Microcavity fabrication
Fabrication material	Silicon Dioxide Fused quartz target	Kurt J. Lesker Company	EJUSIO2451	Microcavity fabrication
Chemical	Nusil®Gel8100	Nusil		Microcavity fabrication
Chemical	Sygard®527	Dowsil		Microcavity fabrication
Chemical	Sylgard®184	Dowsil		Microcavity fabrication

Chemical	Ethyl butanoate	VWR		Retaining animals within field of view
Chemical	Mineral (Paraffin) oil	VWR		Suspension of ethyl butanoate
Fabrication material	24 mm^2 glass substrate			Microcavity fabrication
Equipment	FlexAFM	Nanosurf		Atomic force microscope
Equipment	uniqprobe™ Cantilevers	Nanosensors	qp-CONT	Stiffness calibration by Atomic Force Microscopy
Equipment	CM110 Monochromator	Spectral Products		Monochromator for scanning wavelength ERISM
Equipment	Optical cage system components	Thorlabs		Cage system for ERISM and WARP, see supplementary information.
Equipment	EMS 6000 Photoresist Spincoater	Electronic Microsystems	EMS 6000	Microcavity fabrication
Equipment	Ultra high vacuum deposition chamber	Ångstrom Engineering		Microcavity fabrication
Equipment	Andor Zyla 4.2 10-Tap	Andor Technology		WARP and ERISM image acquisition
Equipment	iCube CMOS	NET GmbH	NS4203BU	Brightfield image acquisition
Equipment	XIMEA CMOS	XIMEA GmbH	MQ013MG-E2	Behavioural image acquisition
Chemical	CHAPS, 3-[(3-cholamidopropyl)dimethyl ammonio]-1-propane sulfonate			Electrostatic buffer for atomic force microscopy measurements

Animal Rearing

Animals were raised on standard cornmeal and yeast medium (17.4 g/L yeast, 73.1 g/L cornmeal, 5.8 g/L agar, 4.8 ml/L propionate) at 25°C with a 12-hour light-dark cycle except where explicitly stated otherwise. Animals were given at least 1 hour to acclimate to room temperature prior to all experiments. Immediately prior to experiments, samples of media containing larvae were taken using a spatula before being placed into a columnar stacked sieve with 40, 60 and 100 meshes from top to bottom, respectively. Media samples were run under gentle flowing tap water to separate adult debris, 2^{nd} instar larvae and 1^{st} instar larvae with embryos on each mesh. Larvae from the 60-mesh fraction of the sieve were observed under a microscope and animals around 1 mm were selected and washed before being placed on 1% (w/v) agarose lined dishes.

Microcavity fabrication

The fabrication protocol of elastic microcavities was adapted from (58). 24 mm^2 borosilicate glass substrates of No.5 thickness were cleaned via ultrasonication in acetone followed by propan-2-ol for 3 minutes. After cleaning, substrates were dried using N_2 and baked at 125°C for 10 minutes to clear any residual solvent. Cleaned glass substrates were then plasma treated with oxygen plasma for 3 minutes at 20 SCCM O_2 flow rate to clear any residual organics and activate the surface of the glass. Cleaned and activated glass substrates were then sputter coated with 0.5nm of Cr, which acted as an adhesion layer for the subsequent 10nm Au layer which was deposited by thermal vapour deposition. 50nm of SiO_2 was then deposited by sputter coating to improve stability of the resultant bottom mirrors. Roughly 100µl of pre-mixed and degassed polydimethylsiloxane gels was spincoated onto the bottom mirrors at 3000RPM, 1500RPM acceleration, for 60 seconds and then quickly transferred to a pre-heated metal plate at 150°C for 1.5 hr to cure the elastomer. After curing, elastomer coated bottom mirrors were O_2 plasma treated with the desired plasma power at 20 SCCM O_2 flow rate for 10 seconds. 15nm of Au was then deposited onto the oxidised elastomer, thus completing the microcavity.

Microcavity characterisation

Microcavities were characterised using a NanoSurf Flex Atomic Force Microscope (Nanosurf, Liestal, Switzerland). 15-18µm diameter glass beads were glued to the tip of Uniqprobe™ QPCont cantilevers (Nanosensors AG, Neuchatel, Switzerland) using a UV-polymer glue after thermal calibration of the spring constant at 21°C. Sphere-tipped cantilevers were then indented into microcavity samples at 1µm/s with up to 30nN of force. This process was repeated across the surface of the microcavity at least 5 times, with each measurement being roughly 2mm apart to get a measure of the variation across the cavity surface. Force-distance profiles recorded by the AFM were then fitted to the Hertz model to compute the Young's modulus at each point of each sample. Mean cavity lengths were measured by taking 4 ERISM images at 4x magnification from each corner of the cavity, and then taking the mean of 4 regions of interest per image.

Prior to use in experiments, a 12-well silicone chamber (ibidi GmbH, Munich, Germany) was cut such that only 1 large square-well, originally comprised of four smaller wells cut off from the rest of the chamber, remained and was placed onto a microcavity. A low pH Collagen-I (1mg/ml; Millipore L7220) solution was then prepared at a 1:1 (v/v) ratio with pH3 phosphate buffered saline (PBS). pH3 PBS was prepared with either hydrochloric acid or acetic acid, mixing until pH3 was recorded using an electronic pH meter. Collagen-I mixtures were then dosed onto microcavities in silicone wells (1ml per microcavity) and allowed to coat the surface overnight at 4°C. Immediately before the experiment, microcavities were washed with deionised water at least 5 times, taking care not to remove all liquid to prevent damage to the top gold surface.

Denticle band kinematic imaging

All animals were raised in ambient light conditions at room temperature. Between 48 and 72 hours after flies were introduced to fresh media, feeding 2nd instar Canton-S wildtype animals were selected with a size exclusion criterion - any animals below 0.8 mm or above 1.5 mm were rejected. Animals were then washed and allowed to acclimate to 0.5% (w/v) agarose.

Immediately before experiments, a single animal was transferred to a freshly set dish containing 0.5% (w/v) agarose while still transparent. These dishes were then quickly placed onto the 3D printed stage of a custom-built inverted Bresser Advance ICD stereomicroscope (Bresser GmbH, Rhede, Germany). Denticle band images were acquired, through the still transparent agarose substrate, at 60 frames per second for at least 1 minute while the larva was freely behaving. All images were acquired using a XIMEA CMOS camera (XIMEA GmBH, Münster, Germany) through MicroManager 1.4 (59). The velocity of 33 individual identifiable points across the animal's body during peristaltic waves whilst imaging from the ventral side of 2nd instar larvae Denticle bands were tracked manually using the Manual Tracking plugin of ImageJ (60). Analysis of tracking data was performed using OriginPro 2019 (OriginLab Corporation, MA, USA).

ERISM and WARP imaging

Elastic Resonator Interference Stress microscopy (ERISM) was used to record high-resolution maps of substrate indentations by monitoring local changes in the resonances of a soft and deformable optical microcavity. ERISM has been used to quantify cellular forces down to the piconewton range. The static thickness of microcavities was measured adapting our previously published ERISM method as described in (24,58). In brief, images of the cavity were taken under epi-illumination with a series of 201 different wavelengths (550-750nm in 1nm steps). From these images, the minima in the spectral reflection for each pixel were correlated with theoretical values obtained from optical modelling for cavities of different thicknesses to determine the actual thickness at each position across the image (Cavities were between 8-12µm in static thickness.) Thickness maps were converted into maps of local displacement by subtracting a linear plane, using the mean thickness of the cavity in each corner.

For dynamic force mapping, we used a further improved version of the WARP routine described in (26). Epi-illumination with light of two different and quickly alternating wavelengths was produced by passing the emission from two identical red LEDs (dominant emission wavelength 625nm, FWHM 17nm; Thorlabs Inc. NJ, USA) through two identical narrow bandpass filters (peak transmission at 633nm, FWHM of 1nm; Thorlabs Inc., NJ, USA). By tilting the filter located in front of one of the LEDs by approximately 15 degrees relative to the incident light, its peak transmission wavelength was tuned to λ_θ=628nm. For the optical modes supported by our microcavities, this corresponds to a phase shift of roughly 90°, but remains within the same free spectral range band of the cavity. For the WARP measurements, we first took calibration images (under subsequent illumination at λ and λ_θ) of the empty microcavity in an area with roughly linear slope in cavity thickness, e.g. near where the silicone well containing the larvae meets the surface of the cavity. Images of behaving larvae were then recorded under rapidly alternating illumination at λ and λ_θ, with the camera sending alternating trigger pulses to each LED to generate interleaved stacks of λ and λ_θ images.

Displacement maps were obtained from these stacks using a series of image transformations, based around the fact that the ratio of the difference and the sum of pixel intensities at λ and λ_θ is linked to local thickness in an unambiguous manner, at least across each free spectral range. See Supporting Information Fig. S4 and (26) for further details on the calculation of displacement from the λ and λ_θ images. All WARP and ERISM images were acquired using an Andor Zyla 4.2 sCMOS camera (Andor Technology, Belfast, UK).

Stress maps were calculated from the ERISM and WARP displacement maps as described previously (23), using a finite element method simulation via COMSOL multiphysics (COMSOL Ltd., Cambridge, UK) and the known mechanical properties of the microcavity.

Polydimethylsiloxane gel preparation

Polydimethylsiloxane elastomers were prepared according to manufacturer guidelines for all gels. The two component precursors of different gels were mixed together in separate glass bottles, using an equal mass ratio of the two components for Sylgard 527 and NulSil Gel8100 but a 1:10 volumetric ratio for Sylgard 184. Mixing was performed by 10 min of magnetic stirring (Sylgard 527 and NuSil GEL8100) or by 10 min of mechanical stirring (Sylgard 184). The elastomer mixtures were then combined in a fresh bottle in the desired mass ratio using a syringe following the same method as a previous study (44). Combined elastomers were mixed for a further 10 minutes. Mixtures containing Sylgard®184 were initially mixed by high speed vortexing to coarsely disperse the gel to allow for the magnetic stir bar to overcome the high viscosity of the gel. After mixing, all preparations were degassed under vacuum for around 5 minutes, prior to fabrication of microcavities.

Anaesthetised animal force imaging

Animals were selected, cleaned, and placed in a fridge at 4°C for 2-3 hours to anaesthetise them. Immediately prior to experiments, anaesthetised animals were gently placed onto a collagen coated microcavity in a petri-dish on ice. The microcavities were then placed, using a moistened paint brush, on the ERISM-WARP microscope and the animals were observed carefully. As soon as mouth-hook movement was observed, an ERISM measurement was taken. Animals often had to be placed back onto ice to anaesthetise them once more as they rapidly regained motility. As the complete ERISM scan requires ca. 5 seconds, animals were required to be completely stationary in order to obtain reliable stress map images.

Freely behaving animals force imaging

Animals were selected according to the previously outlined criteria and cleaned before being placed onto a 1% (w/v) agarose lined petri dish. Elastic resonators were prepared according to the coating criteria mentioned above. 10% Nusil®GEL8100, 180W O_2 plasma treated microcavities were used for all freely behaving experiments. Once calibration images of the microcavity were acquired, excess water was removed from the cavity and animals were gently placed onto the cavity surface with a paintbrush, taking care to ensure there was enough moisture on the animal to prevent drying by wetting the paintbrush prior to transferring the animal. In order to keep animals on the sensor surface, a 50µl drop of 15mM ethyl butanoate (Sigma-Aldrich Inc., MO, USA), suspended in paraffin oil, was dropped onto a 24 mm^2 glass coverslip before being inverted and placed on top of the silicone well (ibidi GmbH, Munich, Germany) such that the attractive odorant faced towards the animal but perpetually out of its reach. Animal substrate interaction was then imaged by WARP, using alternating wavelengths to generate a series of interleaved cavity resonance images, and displacement and stress maps were generated as described prior. All WARP videos were recorded at 120FPS, producing displacement maps with an effective framerate of 60FPS, using a 4X magnification objective. Due to the high framerate, we were limited to the use of ¼ of the total camera sensor, thus higher magnifications would prevent mapping of the whole-animal.

Statistical Analyses

All statistical analysis was performed using OriginPro 2019 (OriginLab Corporation, MA, USA). Coefficients of determination (R^2) for all but GRF vs contact area analysis were determined using a linear fit. The rarity of backwards waves during normal larval behaviour precluded analysis of latencies as used in **Figure 2**. Adjusted coefficients of determination (Adj. R^2) for the GRF vs contact area analysis was performed using a 2nd order polynomial fit instead as this describes the

data better than a linear fit. Two-way repeated measures ANOVA was used in segmentwise peak contact area analysis, as data were normally distributed according to a Shapiro-Wilk test. However, Levene's test for homogeneity of variances was significant for SI ($p<0.05$) but not for ST ($p=0.092$), we urge caution when interpreting the within-subjects' effects. Mauchly's test showed sphericity of segment ($W=0.082$, $p=0.063$) and the segment*SI-ST interaction ($W=0.27428$, $p=0.62463$), where the SI-ST factor was not tested due to insufficient degrees of freedom. Independent samples t-test was performed to show no significant difference between larval behaviour on elastic resonators and standard agarose substrates as data were normally distributed according to a Shapiro-Wilk test. Pairwise comparisons between segments all used Tukey-corrected t-tests. Force-distance curves were fitted using a height-corrected Hertz Model; all force-distance curves were fitted with an $R^2>0.9$.

Acknowledgements

This work was supported by EPSRC (Doctoral Training grant EP/L505079/1 and grant EP/P030017/1), the European Research Council under the European Union's Horizon 2020 Framework Programme (FP/2014-202) ERC grant agreement no. 640012 (ABLASE), and the Alexander von Humboldt Foundation via the Humboldt Professorship to MCG. We thank our technicians Audrey Grant and Tanya Sneddon for preparing fly food, Dr Eleni Dalaka for her support during atomic force microscopy experiments, Dr Andreas Mischok for his advice with fabrication, Dr Marcus Bischoff for his advice and support early in the work, and Dr Jacob Francis and Dr James MacLeod for their methodological advice regarding lateral view imaging.

Author Contributions

Experiments were conceived and designed by J.H.B., M.C.G. and S.R.P.; fabrication and experiments were performed by J.H.B., method was designed by N.M.K. and A.M.; data analysis was performed by J.H.B., N.M.K. and A.M.; animal rearing was performed by J.H.B. and S.R.P; writing was performed by J.H.B. and S.R.P. with input from by M.C.G., N.M.K. and A.M.

Supplementary Information

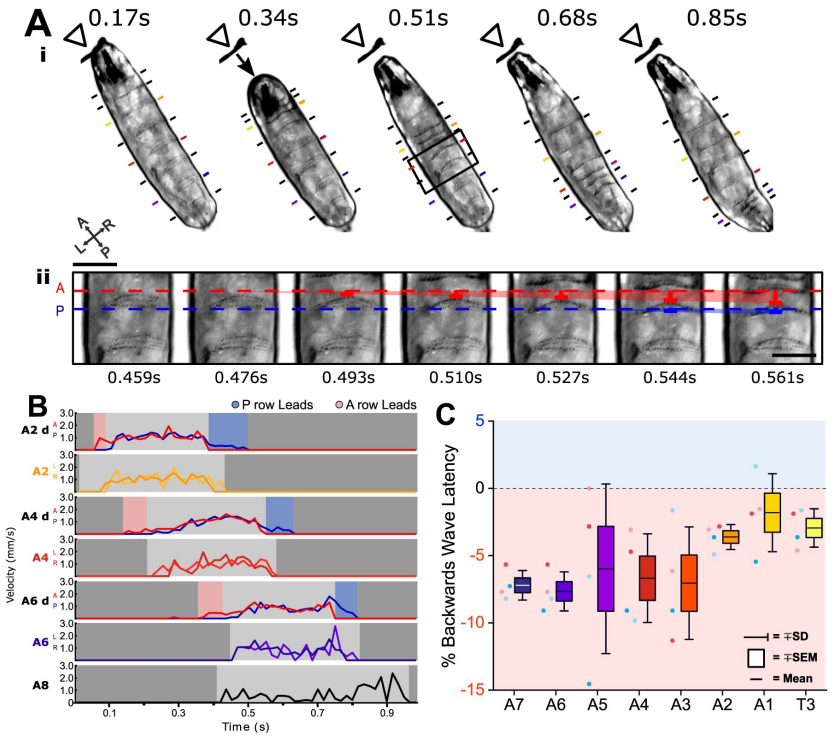

Figure S1.

Backwards waves show a reversed heel toe rule.

A) Backwards waves are characterised by sequential contractions moving from anterior to posterior, the reverse of forwards waves (**i**). We observed that the anterior row of each denticle band moved to meet the posterior row before the whole protopodia began to move (**ii**). **B)** We tracked the velocity of the lateral edge of each denticle band (A6, A4, A2) and the anterior and posterior rows of each denticle band (A6d, A4d, A2d). Similar to forward waves in **Figure 2**, we observed an anteroposterior latency between when each row moved relative to the other. However, this was the reverse of forwards waves, with the swing initiation period being characterised by an anterior-led latency and the swing termination period being characterised by a posterior-led latency. **C)** We found that this was relatively consistent across segments, where negative numbers represent anterior led latency, within a sample of 4 waves across 4 different animals.

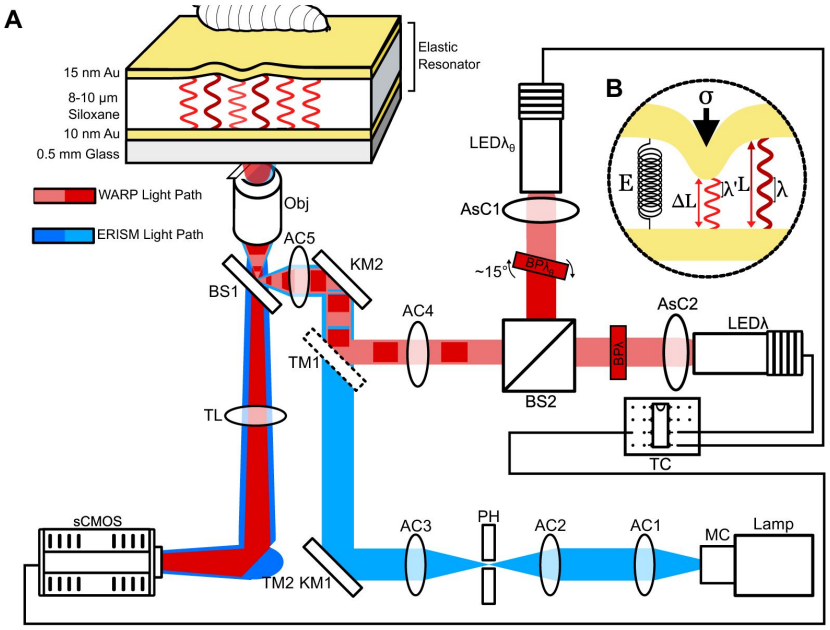

Figure S2.

Optical setup for ERISM and WARP experiments.

A) Optical light path used to record resonance from incident light on elastic resonators. For ERISM (blue), light originates from a halogen lamp (Lamp) and is spectrally scanned by a monochromator (MC) before being collimated by an achromatic doublet lens (AC1) and focused by another achromatic doublet lens (AC2) through a pinhole (PH). Light emerging from PH is then recollimated by AC3 into a kinematic mirror (KM1), directing it to KM2 which then directs the light under the nosewheel of a Nikon Ti2 inverted microscope. Under the nosewheel, the light is focused by an achromatic doublet lens (AC5) to a 50:50 RT beamsplitter plate (BS1), which directs the focused light to the back aperture of the objective (Obj). Light is then introduced onto the elastic resonator via Obj, whereupon it either enters the cavity, should it meet the resonance condition for the given cavity thickness, or is reflected, should it not meet this condition. Reflected light is then collected by Obj, focused by the tubelens (TL) and directed by the microscope turning mirror (TM2) then recorded by a camera (Camera). Though depicted as blue, ERISM typically scans through a spectral band from 550-750 nm. For WARP (red), light is generated by two 625 nm red LEDs (LEDλ and LEDλθ). For both LEDs, the light is collimated by aspheric condenser lenses (AsC1 and AsC2) and is then filtered by 633 nm bandpass filters (BPλ and BPλθ). BPλθ, is rotated roughly 15° such that the filter pass band is blue-shifted and the resultant transmitted light is approximately 90 degrees out of phase (in terms of the resonances of the elastic cavity) relative to light passing through BPλ. These light paths are combined by a beamsplitter cube (BS2) and focused into the KM2, AC4, BS1, Obj common light path by a dielectric turning mirror (TM1) only present when using WARP. The LEDs are then triggered in an alternating pattern by a trigger circuit decade counter (TC) which is controlled by the trigger out of the sCMOS camera. **B)** Working principle within the elastic cavity. When under stress (σ), the elastic cavity deforms from its resting length (L) to its strained length (ΔL). The change in cavity length causes a change in the wavelengths that fulfil the resonance condition of the cavity. The amount of strain under a given stress is a direct consequence of the Young's modulus (E) of the elastic material.

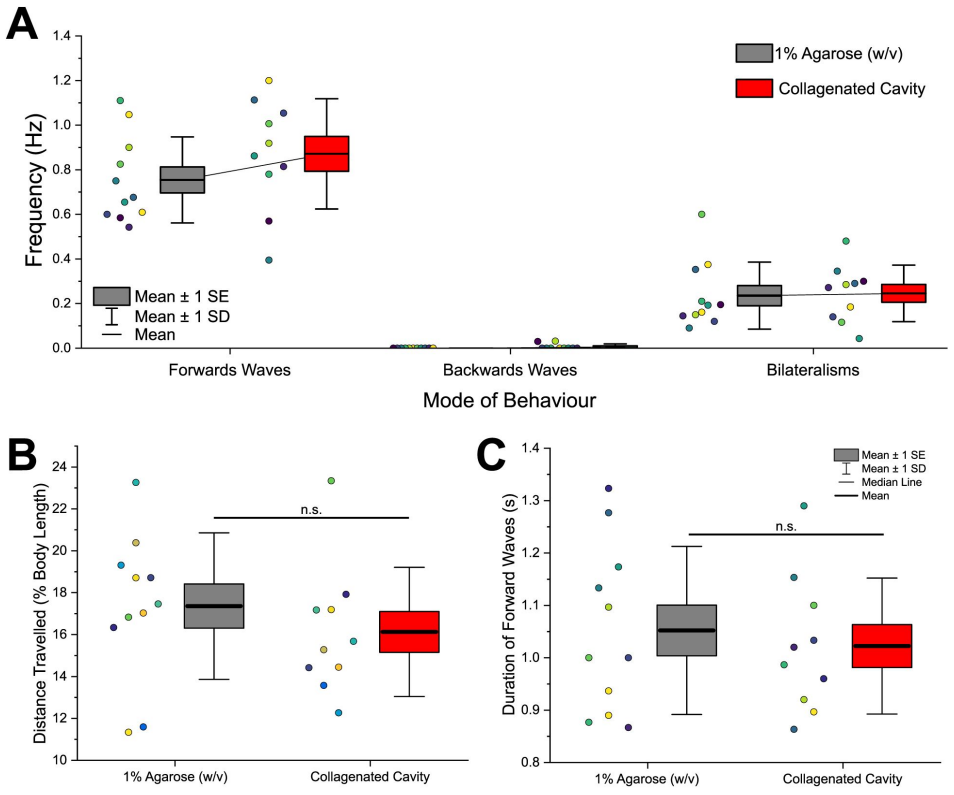

Figure S3.

Ordinary larval behaviour is maintained on collagen treated microcavities as compared to commonly used agarose substrates.

A) Total number of behaviours per second is not significantly different between agarose substrates and elastic cavities with collagen coating according to a two-sample t-test (t(18)=-1.24, p=0.23). Data for forwards waves, backwards waves and head sweep bilateralisms are shown. **B)** Distance travelled as % of body length was not significantly different between the two substrates according to a two-sample t-test (t(18)=1.34, p=0.20). Each data point represents the mean of 5 waves from a single animal. **C)** The mean duration of 5 forwards waves was not significantly different on microcavities compared to agarose according to a two-sample t-test (t(18)=0.62, p=0.54). Data taken from 10 animals. Colour of data point indicates data from an individual animal. All tested data was found to be normally distributed according to a Shapiro-Wilk test (p>0.05).

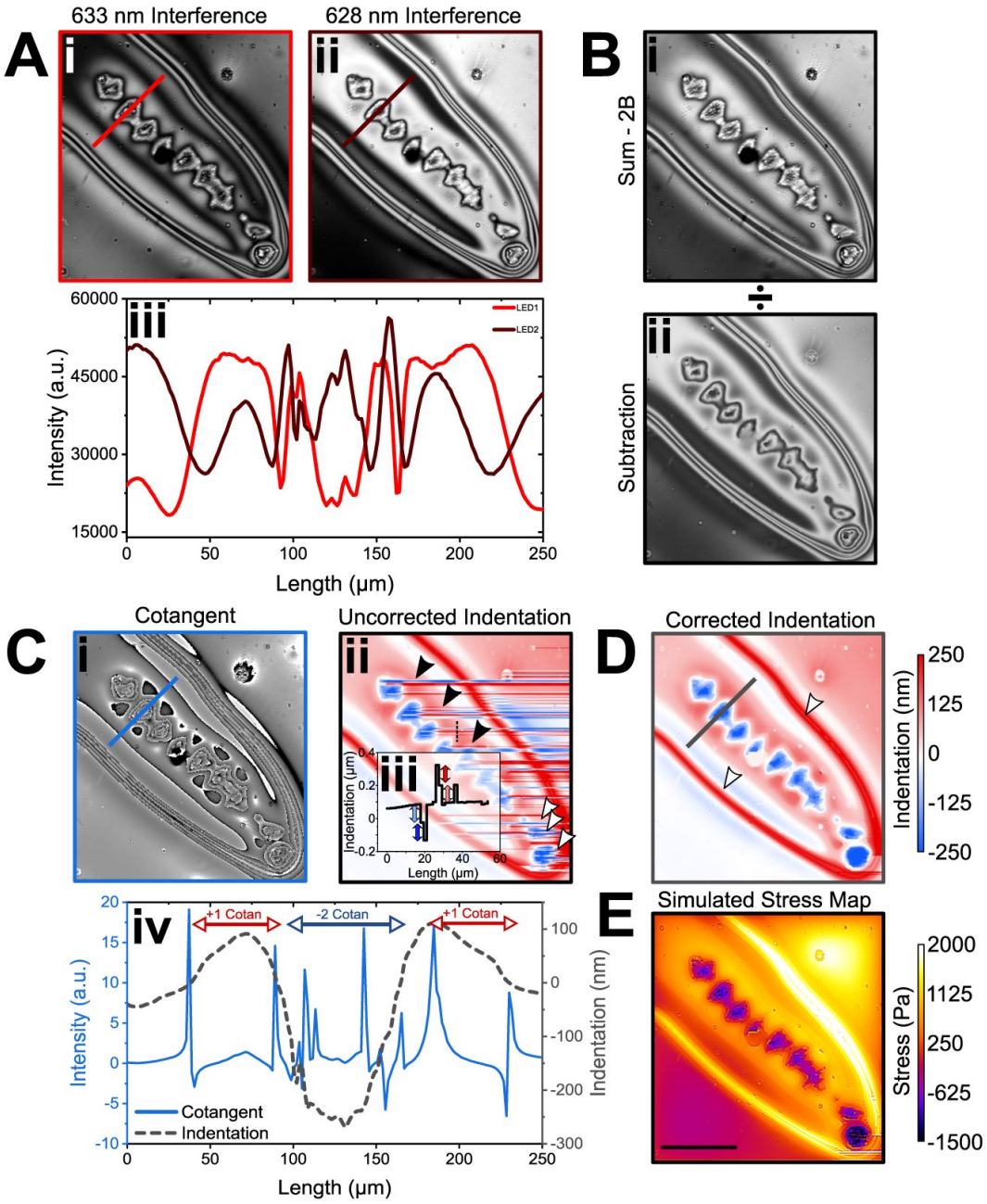

Figure S4.

WARP computation pipeline.

A) Interference images are taken at 633 nm (**i**) and 628 nm (**ii**) in quick alternation. Profile plot (**iii**) across the lines in **i** and **ii**. Note that interference pattern is approximately 90° out of phase relative to the other as a result of the specific wavelength difference and total cavity thickness chosen here. **B)** Images were then added together (**i**) with a background correction (2B) and then divided by the same two images subtracted from each other (**ii**). **C)** The resultant images are referred to as cotangent images as pixel intensity changes approximately as the cotangent of the cavity thickness in these (**i**). A cotangent lookup table was then used to convert 16bit greyscale values in the cotangent images to local cavity length. Raw and uncorrected displacement map computed by subtracting a linear plane of mean cavity thickness (**ii**). Profile plot (**iii**) along the thin dashed line in ii, clearly showing discontinuity artefacts (indicated by blue and red double arrows). These linear artefacts correspond to step heights amounting to jumps by one free spectral range, which was 112 nm in this instance. **D)** Corrected displacement map where the linear artefacts across the image were corrected by applying a continuity condition. **E)** Profile plots of cotangent signal and corrected displacement along the thick lines in **Ci** and **D**. **F)** Stress maps were calculated from the displacement map by FEM using the known mechanical properties of the substrate. Scalebar = 200 μm.

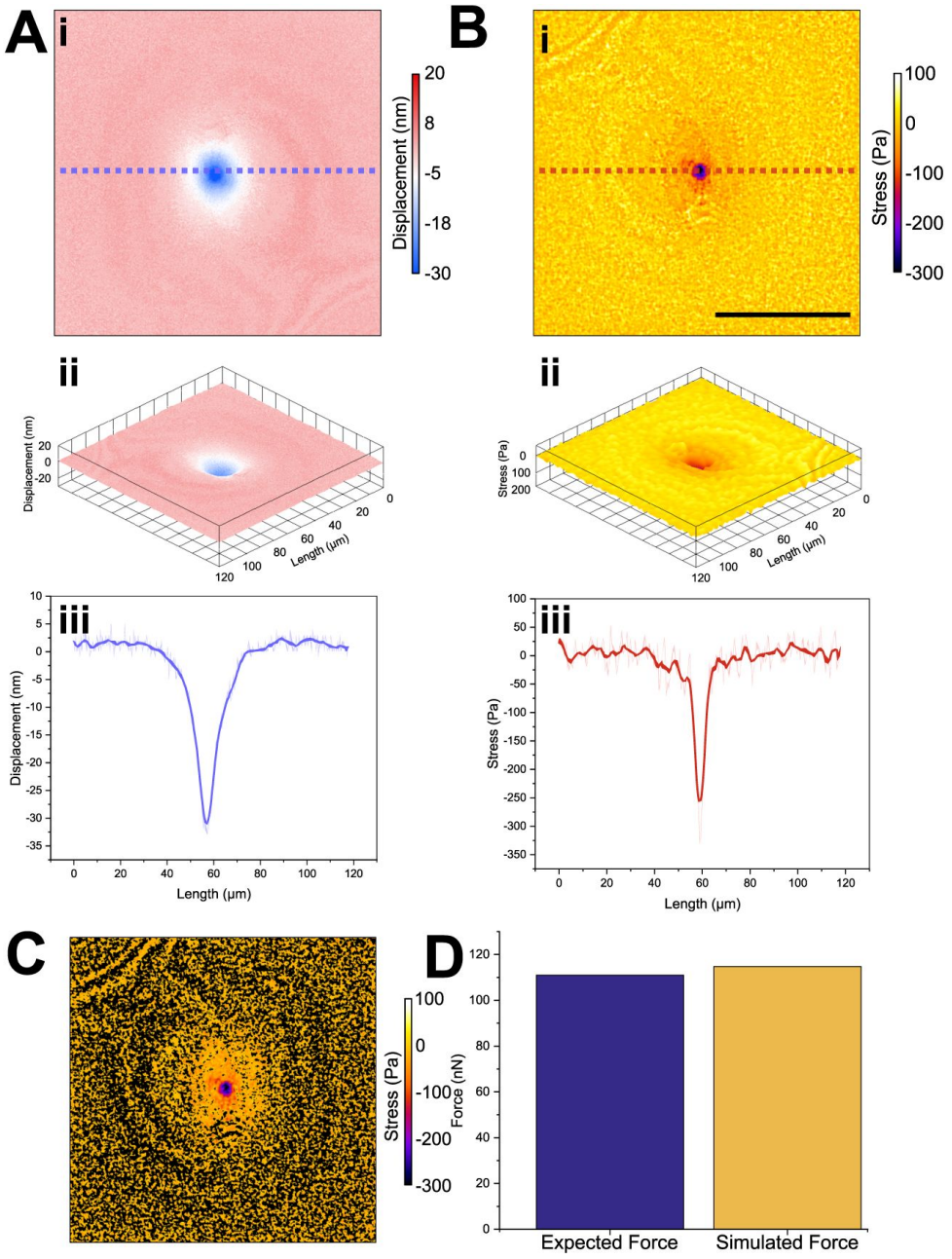

Figure S5.

Confirmation of finite element method (FEM) simulation accuracy.

A) Using atomic force microscopy (AFM), we indented into an elastic resonator made within the same batch as those used for videorate stress mapping. (**i**) False colour map and (**ii**) 3D projection of displacement smoothed by 10 points. (**iii**) Profile along blue dotted line in (**i**) showed that a 111 nN indentation force resulted in a roughly 32 nm peak indentation; data averaged by 10 points, raw data shown in a lighter colour. **B)** Using FEM, we calculated a stress map from the displacement map, using the young's modulus of the bulk material, previously recorded as 16450 Pa by AFM. (**i**) False colour and (**ii**) 3D projection of stress experienced by the resonator smoothed by 10 points (**ii**). Profile along red dotted line in (**i**) showing the peak stress produced by 111 nN of force approximately 320 Pa; data averaged by 10 points, raw data shown in a lighter colour. **C)** We thresholded the resultant simulation to remove all cavity displacements >0nm. **D)** Integration of stress in **C** gives a prediction of the total applied force as determined from displacement map and FEM model, without prior knowledge of the indentation force. Comparing this simulated force to the applied force of 111 nN, we found the relative difference to be only 3.4%, with our simulation estimating a total applied force of 114.8 nN. Scale bar in **B** denotes 50 µm.

Elastomer Mixture	Mean Young's Modulus (Pa)	Plasma power (W)
10% Sylgard®184, 90% Sylgard®527	27697.978 ± 913.45	30
6.6% Sylgard®184, 94.4% Sylgard®527	25999.17 ± 991.93	30
5% Sylgard®184, 95% Sylgard®527	18596.08 ± 186.05	30
100% Sylgard®527	12325.35 ± 395.45	30
100% Nusil®GEL8100	3340.30 ± 53.45	30
10% Sylgard®527, 90% Nusil®GEL8100	8974.32 ± 621.83	180
50% Sylgard®527, 50% Nusil®GEL8100	18404.14 ± 439.85	180
90% Sylgard®527, 10% Nusil®GEL8100	38387.87 ± 2768.63	180

Table S1

Measured effective Young's Modulus per elastomer mixture post plasma treatment.

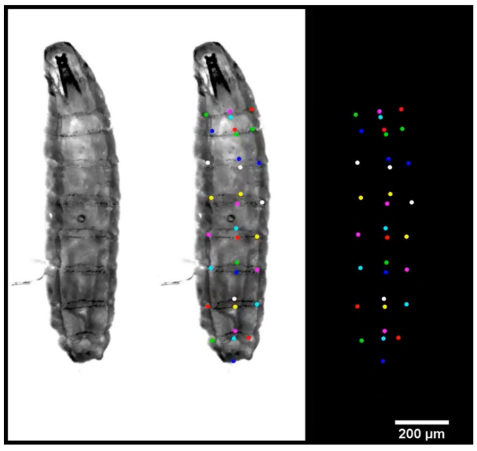

Video SV1.

Kinematic Tracking of Forwards and Backwards Peristaltic waves.

Manual tracking of 33 points across the body during forwards and backwards peristalses.

Video SV2.

Lateral view crawling.

Video showing the sequestration and planting of protopodia during locomotion from a lateral view.

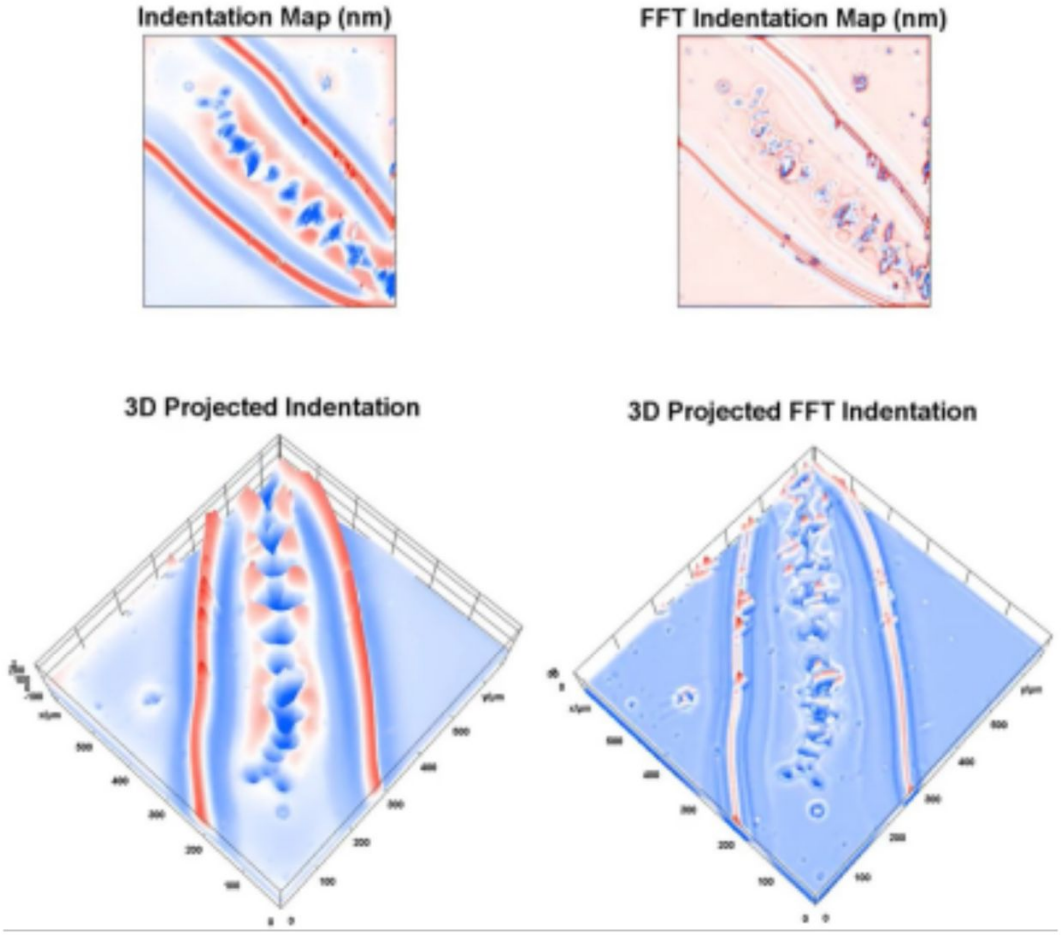

Video SV3.

WARP imaging during forwards peristalses.

Video showing high frame rate displacement maps produced by a freely behaving Drosophila larva. Displacement maps were high-pass Fourier filtered to make denticulated cuticle more readily visible and projected in 3D to show the effects of substrate interaction. Details of the Fourier filtering procedure were described in a previous study (23).

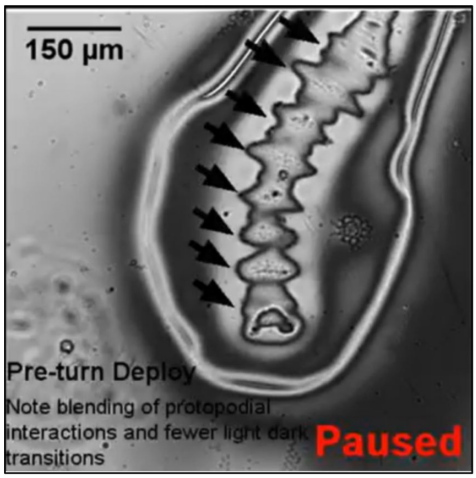

Video SV4.

Interference mapping of bodymass redistribution during anterior bilateral behaviours.

Video showing the raw reflection data during the preparatory phase of bilateral behaviours.

References

1. Audu ML, Kirsch RF, Triolo RJ (2007) **Experimental verification of a computational technique for determining ground reactions in human bipedal stance** *J Biomech* **40**:1115–24

2. van Griethuijsen LI, Trimmer BA (2014) **Locomotion in caterpillars** *Biological Reviews* **89**:656–70

3. Berrigan D, Pepin DJ (1995) **How maggots move: Allometry and kinematics of crawling in larval Diptera** *Journal of Insect Physiology* **41**:329–37

4. Gray J, Lissmann HW (1964) **The Locomotion of Nematodes** *Journal of Experimental Biology* **41**:135–54

5. Bobbert MF, Gómez Alvarez CB, van Weeren PR, Roepstorff L, Weishaupt MA (2007) **Validation of vertical ground reaction forces on individual limbs calculated from kinematics of horse locomotion** *J Exp Biol* **210**:1885–96

6. Trueman ER (1975) **locomotion of soft-bodied animals**

7. Tanaka Y, Ito K, Nakagaki T, Kobayashi R (2012) **Mechanics of peristaltic locomotion and role of anchoring** *Journal of The Royal Society Interface* **9**:222–33

8. Lin HT, Trimmer BA (2010) **The substrate as a skeleton: ground reaction forces from a soft-bodied legged animal** *Journal of Experimental Biology* **213**:1133–42

9. Lin HT, Trimmer BA (2012) **A new bi-axial cantilever beam design for biomechanics force measurements** *Journal of Biomechanics* **45**:2310–4

10. Lin HT, Slate DJ, Paetsch CR, Dorfmann AL, Trimmer BA (2011) **Scaling of caterpillar body properties and its biomechanical implications for the use of a hydrostatic skeleton** *Journal of Experimental Biology* **214**:1194–204

11. Cacciatore TW, Rozenshteyn R, Kristan WB (2000) **Kinematics and Modeling of Leech Crawling: Evidence for an Oscillatory Behavior Produced by Propagating Waves of Excitation** *J Neurosci* **20**:1643–55

12. Kampowski T, Eberhard L, Gallenmüller F, Speck T, Poppinga S (2016) **Functional morphology of suction discs and attachment performance of the Mediterranean medicinal leech (Hirudo verbana Carena)** *Journal of The Royal Society Interface* **13**

13. Fang-Yen C, Wyart M, Xie J, Kawai R, Kodger T, Chen S, et al. (2010) **Biomechanical analysis of gait adaptation in the nematode Caenorhabditis elegans** *Proceedings of the National Academy of Sciences* **107**:20323–8

14. Gjorgjieva J, Biron D, Haspel G (2014) **Neurobiology of Caenorhabditis elegans Locomotion: Where Do We Stand?** *BioScience* **64**:476–86

15. Krieg M, Fläschner G, Alsteens D, Gaub BM, Roos WH, Wuite GJL, et al. (2019) **Atomic force microscopy-based mechanobiology** *Nat Rev Phys* **1**:41–57

16. Mohammed D, Versaevel M, Bruyère C, Alaimo L, Luciano M, Vercruysse E, et al. (2019) **Innovative Tools for Mechanobiology: Unraveling Outside-In and Inside-Out Mechanotransduction**

17. Zancla A, Mozetic P, Orsini M, Forte G, Rainer A (2022) **A primer to traction force microscopy** *Journal of Biological Chemistry* **298**

18. Lekka M, Gnanachandran K, Kubiak A, Zieliński T, Zemła J (2021) **Traction force microscopy – Measuring the forces exerted by cells** *Micron* **150**

19. Yang Z, Lin JS, Chen J, Wang JHC (2006) **Determining substrate displacement and cell traction fields—a new approach** *Journal of Theoretical Biology* **242**:607–16

20. Li D, Colin-York H, Barbieri L, Javanmardi Y, Guo Y, Korobchevskaya K, et al. (2021) **Astigmatic traction force microscopy (aTFM)** *Nat Commun* **12**

21. Schoen I, Hu W, Klotzsch E, Vogel V (2010) **Probing Cellular Traction Forces by Micropillar Arrays: Contribution of Substrate Warping to Pillar Deflection** *Nano Lett* **10**:1823–30

22. Gupta M, Kocgozlu L, Sarangi BR, Margadant F, Ashraf M, Ladoux B, Paluch EK (2015) **Chapter 16 - Micropillar substrates: A tool for studying cell mechanobiology** *Methods in Cell Biology [Internet]*

23. Kronenberg NM, Liehm P, Steude A, Knipper JA, Borger JG, Scarcelli G, et al. (2017) **Long-term imaging of cellular forces with high precision by elastic resonator interference stress microscopy** *Nat Cell Biol* **19**:864–72

24. Liehm P, Kronenberg NM, Gather MC (2018) **Analysis of the Precision, Robustness, and Speed of Elastic Resonator Interference Stress Microscopy** *Biophys J* **114**:2180–93

25. Dalaka E, Kronenberg NM, Liehm P, Segall JE, Prystowsky MB, Gather MC (2020) **Direct measurement of vertical forces shows correlation between mechanical activity and proteolytic ability of invadopodia** *Science Advances* **6**

26. Meek AT, Kronenberg NM, Morton A, Liehm P, Murawski J, Dalaka E, et al. (2021) **Real-time imaging of cellular forces using optical interference** *Nat Commun* **12**

27. Fushiki A, Zwart MF, Kohsaka H, Fetter RD, Cardona A, Griffith LC (2016) **Nose A. A circuit mechanism for the propagation of waves of muscle contraction in Drosophila** *eLife* **5**

28. Zwart MF, Pulver SR, Truman JW, Fushiki A, Fetter RD, Cardona A, et al. (2016) **Selective Inhibition Mediates the Sequential Recruitment of Motor Pools** *Neuron* **91**:615–28

29. Schneider-Mizell CM, Gerhard S, Longair M, Kazimiers T, Li F, Zwart MF, et al. **Quantitative neuroanatomy for connectomics in Drosophila**

30. Pulver SR, Bayley TG, Taylor AL, Berni J, Bate M, Hedwig B (2015) **Imaging fictive locomotor patterns in larval Drosophila** *Journal of Neurophysiology* **114**:2564–77

31. Heckscher ES, Lockery SR, Doe CQ (2012) **Characterization of Drosophila Larval Crawling at the Level of Organism, Segment, and Somatic Body Wall Musculature** *J Neurosci* **32**:12460–71

32. Brand AH, Perrimon N (1993) **Targeted gene expression as a means of altering cell fates and generating dominant phenotypes** *Development* **118**:401–15

33. Payre F (2003) **Genetic control of epidermis differentiation in Drosophila** *Int J Dev Biol* **48**:207–15

34. Loveless J, Lagogiannis K, Webb B (2019) **Modelling the mechanics of exploration in larval Drosophila** *PLOS Computational Biology* **15**

35. Loveless J, Garner A, Issa AR, Roberts RJV, Webb B, Prieto-Godino LL, et al. (2021) **A physical theory of movement in small animals [Internet]**

36. Gjorgjieva J, Berni J, Evers JF, Eglen S (2013) **Neural circuits for peristaltic wave propagation in crawling Drosophila larvae: analysis and modeling**

37. Khare SM, Awasthi A, Venkataraman V, Koushika SP (2015) **Colored polydimethylsiloxane micropillar arrays for high throughput measurements of forces applied by genetic model organisms** *Biomicrofluidics* **9**

38. Sun X, Liu Y, Liu C, Mayumi K, Ito K, Nose A, et al. (2022) **A neuromechanical model for Drosophila larval crawling based on physical measurements** *BMC Biology* **20**

39. Tytell ED, Holmes P, Cohen AH (2011) **Spikes alone do not behavior make: why neuroscience needs biomechanics** *Curr Opin Neurobiol* **21**:816–22

40. Federle W, Labonte D **Dynamic biological adhesion: mechanisms for controlling attachment during locomotion**

41. Ahearne M, Yang Y, El Haj AJ, Then KY, Liu KK (2005) **Characterizing the viscoelastic properties of thin hydrogel-based constructs for tissue engineering applications** *J R Soc Interface* **2**:455–63

42. Salerno M, Dante S, Patra N, Diaspro A (2010) **AFM measurement of the stiffness of layers of agarose gel patterned with polylysine** *Microsc Res Tech* **73**:982–90

43. Apostolopoulou A, Hersperger F, Mazija L, Widmann A, Wüst A, Thum A (2014) **Composition of agarose substrate affects behavioral output of Drosophila larvae** *Frontiers in Behavioral Neuroscience [Internet* **8**

44. Palchesko RN, Zhang L, Sun Y, Feinberg AW (2012) **Development of Polydimethylsiloxane Substrates with Tunable Elastic Modulus to Study Cell Mechanobiology in Muscle and Nerve** *PLOS ONE* **7**

45. Dimitriadis EK, Horkay F, Maresca J, Kachar B, Chadwick RS (2002) **Determination of Elastic Moduli of Thin Layers of Soft Material Using the Atomic Force Microscope** *Biophysical Journal* **82**:2798–810

46. Pritchard R H., Lava P, Debruyne D, Terentjev E M. (2013) **Precise determination of the Poisson ratio in soft materials with 2D digital image correlation** *Soft Matter* **9**:6037–45

47. Fitzpatrick MJ, Szewczyk E (2005) **Locomotion is not influenced by denticle number in larvae of the fruit fly Drosophila melanogaster** *Can J Zool* **83**:368–71

48. Burnette DT, Shao L, Ott C, Pasapera AM, Fischer RS, Baird MA, et al. (2014) **A contractile and counterbalancing adhesion system controls the 3D shape of crawling cells** *Journal of Cell Biology* **205**:83–96

49. Friesen K, Chen H, Zhu J, Taylor DB (2015) **External Morphology of Stable Fly (Diptera: Muscidae) Larvae** *Journal of Medical Entomology* **52**:626–37

50. Simon MA, Fusillo SJ, Colman K, Trimmer BA (2010) **Motor patterns associated with crawling in a soft-bodied arthropod** *Journal of Experimental Biology* **213**:2303–9

51. Vaadia RD, Li W, Voleti V, Singhania A, Hillman EMC, Grueber WB (2019) **Characterization of Proprioceptive System Dynamics in Behaving Drosophila Larvae Using High-Speed Volumetric Microscopy** *Curr Biol* **29**:935–944

52. Ormerod KG, Scibelli AE, Littleton JT (2022) **Regulation of excitation-contraction coupling at the Drosophila neuromuscular junction** *The Journal of Physiology* **600**:349–72

53. Budd GE (2001) **Why are arthropods segmented?** *Evol Dev* **3**:332–42

54. Card G, Dickinson MH (2008) **Visually Mediated Motor Planning in the Escape Response of Drosophila** *Current Biology* **18**:1300–7

55. Watanabe R, Higuchi T (2022) **Anticipatory action planning for stepping onto competing potential targets**

56. Zanini R, Deprá M, Valente V (2016) **Ultrastructural characterization of the pre-adult stages of Drosophila willistoni species group (Diptera** *Drosophilidae). Trends in Entomology* **12**:43–50

57. Valentine JW (1989) **Bilaterians of the Precambrian—Cambrian transition and the annelid—arthropod relationship** *Proc Natl Acad Sci U S A* **86**:2272–5

58. Kronenberg NM, Gather MC, Liehm P (2017) **Fabrication of elastic micro-cavity chips for use in Elastic Resonator Interference Stress Microscopy**

59. Edelstein A, Amodaj N, Hoover K, Vale R, Stuurman N (2010) **Computer Control of Microscopes Using μManager** *Current Protocols in Molecular Biology* **92**:14–14

60. Schindelin J, Arganda-Carreras I, Frise E, Kaynig V, Longair M, Pietzsch T, et al. (2012) **Fiji: an open-source platform for biological-image analysis** *Nat Methods* **9**:676–82

Article and author information

Jonathan H. Booth
SUPA, School of Physics and Astronomy, University of St Andrews, Fife, United Kingdom, Humboldt Centre for Nano- and Biophotonics, Department of Chemistry, University of Cologne, Germany;, School of Psychology and Neuroscience, University of St Andrews, Fife, United Kingdom
ORCID iD: 0000-0002-9198-226X

Andrew T. Meek
SUPA, School of Physics and Astronomy, University of St Andrews, Fife, United Kingdom, Humboldt Centre for Nano- and Biophotonics, Department of Chemistry, University of Cologne, Germany;

Nils M. Kronenberg
SUPA, School of Physics and Astronomy, University of St Andrews, Fife, United Kingdom, Humboldt Centre for Nano- and Biophotonics, Department of Chemistry, University of Cologne, Germany;
ORCID iD: 0000-0001-6386-3848

Stefan R. Pulver
School of Psychology and Neuroscience, University of St Andrews, Fife, United Kingdom
For correspondence: sp96@st-andrews.ac.uk
ORCID iD: 0000-0001-5170-7522

Malte C. Gather
SUPA, School of Physics and Astronomy, University of St Andrews, Fife, United Kingdom, Humboldt Centre for Nano- and Biophotonics, Department of Chemistry, University of Cologne, Germany;
For correspondence: mcg6@st-andrews.ac.uk
ORCID iD: 0000-0002-4857-5562

Copyright

Editors

Reviewing Editor
Julijana Gjorgjieva
Technical University of Munich, Freising, Germany

Senior Editor
Claude Desplan
New York University, New York, United States of America

Reviewer #1 (Public Review):

This work demonstrates a new technique to characterize the interaction between a crawling larva and the substrate on which it is crawling, at much higher temporal speed and spatial resolution than previously possible. While I have some questions about the interpretation of the data, both the demonstration of WARP microscopy to characterize small animal behavior and the discovery of new crawling-associated anatomical features and motor patterns make the paper worthy of attention.

I thank the authors for providing data underlying the figures. In these uncropped data sets, the deformation of the substrate due to the surface tension of an adhering water layer is visible. I would hope the authors would provide a subset of these images and some of the

accompanying information (e.g. that the deformation of the gel due to the water layer cannot be accurately calculated due to too-rapid phase wrapping in the interferogram) as supplements to the text, to aid in interpretation and understanding of the data. It is also worth noting that in the data provided, under the larva, the integral of the stress on the gel is upward, despite the downward force exerted by the protopodia.

Future work using this exciting technique might address the role of surface tension and the balance of forces and might also produce direct evidence to show that the protopodia serve to "anchor" segments of the larva not in motion. Indeed, the most exciting aspect of this work is the number of new questions it both raises and provides a technological pathway towards resolving.

https://doi.org/10.7554/eLife.87746.2.sa1

Reviewer #2 (Public Review):

The biology and dynamics is well-described. The ERISM and WARP methods are state-of-the-art. The most important new information is the highly accurate and detailed maps of displacement. The real achievements are the new locomotory dynamics uncovered with amazing displacement measurements. One key discovery is the broad but shallow anchoring of the posterior body when the anterior body undertakes a "head sweep". Another discovery is the tripod indentation at the tail at the beginning of peristalsis cycles. This paper describes the detailed dynamics of anchoring for the first time. Anchoring behavior now has to be included in the motor sequence for Drosophila larva locomotion in any comprehensive biomechanical or neural model.

https://doi.org/10.7554/eLife.87746.2.sa0

Author Response

The following is the authors' response to the original reviews.

> ***Reviewer #1 (Public Review):***
>
> *(1.1) This work introduces a new method of imaging the reaction forces generated by small crawling organisms and applies this method to understanding locomotion of Drosophila larva, an important model organism. The force and displacement data generated by this method are a qualitative improvement on what was previously available for studying the larva, improving simultaneously the spatial, temporal, and force resolution, in many cases by an order of magnitude. The resulting images and movies are quite impressive.*

We thank the reviewer for their recognition of the achievements our work presents and for their feedback with regard to what they consider our most important findings and the points raised in their review. We will address these points individually below.

> *(1.2) As it shows the novel application of recent technological innovations, the work would benefit from more detail in the explanation of the new technologies, of the rationales underlying the choice of technology and certain idiosyncratic experimental details, and of the limitations of the various techniques. In the methods, the authors need to be sure to provide sufficient detail that the work can be understood and replicated. The description of the results and the theory of motion developed here focus only on forces generated when the larva pushes against the substrate and ignores the equally strong adhesive forces pulling the larva onto the substrate.*

As the reviewer correctly points out, our present work adapts a recently developed set of methods (namely, ERISM and WARP) for use with small soft-bodied animals. The foundational methods have been described in detail in previous publications (refs, 23 and 26). However, upon reflection, we agree that more information can be provided to ensure our work is more accessible and reproducible. We also agree that some additional clarifying information on our approach could be helpful. We have addressed this in the following ways:

(1) We have included a detailed Key Resources table in the methods section to allow for maximum transparency on equipment and reagent sourcing. This can now be found on Pages 16-19.

(2) We have modified the 'Freely behaving animals force imaging' section of the Materials and Methods section to include more detailed information on practical aspects of conducting experiments. These changes can be found on page 23-24 (lines 566–567, 571-577).

(3) We have re-ordered the Materials and Methods section, such that microcavity fabrication and microcavity characterisation occur prior to the description of ERISM and WARP experiments - this change should hopefully aid replication. Details regarding the application of a silicone well to the surface of microcavities have also been added (lines 472-474).

(4) We have added additional text in the Introduction and Results (Pages 3-4 and 7, lines 56-86, and 152-153) to explain our rationale for using ERISM/WARP and additional text in the discussion that discusses the potential role(s) of adhesive forces in larval locomotion (Page 12, lines 301307).

> *(1.3) The substrate applies upward, downward, and horizontal forces on the larva, but only upward and downward forces are measured, and only upward forces are considered in the discussions of "Ground Reactive Forces." An apparent weakness of the WARP technique for the study of locomotion is that it only measures forces perpendicular to the substrate surface ("vertical forces" in Meek et al.), while locomotion requires the generation of forces parallel to the substrate ("horizontal forces"). It should be clarified that only vertical forces are studied and that no direct information is provided about the forces that actually move the larva forward (or about the forces which impede this motion and are also generated by the substrate). Along with this clarification, it would be helpful to include a discussion of other techniques, especially micropillar arrays and traction force microscopy, that directly measure horizontal forces and of why these techniques are inappropriate for the motions studied here.*

We attempted to provide a streamlined Introduction in our initial submission and then compared ERISM/WARP to other methods in our discussion. We are happy to provide a brief overview of substrate force measurement methods in the introduction to help set the stage for readers. The Introduction section of our revised manuscript now contains the following comparison of different mechanobiological imaging techniques on pages 3-4 lines 56-86:

'However, in the field of cellular mechanobiology, many new force measuring techniques have been developed which allow measurement of comparatively small forces from soft structures exhibiting low inertia (15–17) often with relatively high spatial-resolution. Early methods such as atomic force microscopy required the use of laser-entrained silicon probes to make contact with a cell of interest (15). This approach is problematic for studying animal behaviour due to the risk of the laser and probe influencing behaviour. Subsequently, techniques have been developed which allow indirect measurement of substrate interactions. One such approach is Traction Force Microscopy (TFM) in which the displacement of fluorescent markers suspended in a material with known mechanical properties relative to a zero-force reference allows for indirect measurement of horizontally aligned traction forces (17–19). This technique allows for probe-free measurement of forces, but the need to obtain a

precise zero-force reference would make time-lapse measurements on behaving animals challenging; further, depending on the version used, it has insufficient temporal resolution for the measurement of forces produced by many behaving animals, despite recent improvements (20). A second approach revolves around the use of micropillar arrays; in this technique, horizontally-aligned traction forces are measured by observing the deflection of pillars made of an elastic material with known mechanical properties. This approach can be limited in spatial resolution and introduces a non-physiological substrate that may influence animal behavior (21,22).

Recently we have introduced a technique named Elastic Resonator Interference Stress Microscopy (ERISM) which allows for the optical mapping of vertically aligned GRFs in the pico and nanonewton ranges with micrometre spatial resolution by monitoring local changes in optical resonances of soft and deformable microcavities. This technique allows reference-free mapping of substrate deformations and calculation of vertically directed GRFs; it has been used to study a range of questions related to exertion of cellular forces (23–25). Until recently, this technique was limited by its low temporal resolution (~10s), making it unsuitable for recording substrate interaction during fast animal movements, but a further development of ERISM known as wavelength alternating resonance pressure microscopy (WARP), has been demonstrated to achieve down to 10 ms temporal resolution (26). Given ERISM/WARP allows for probe-free measurement of vertical ground reaction forces with high spatial and temporal resolution, it becomes an attractive method for animal-scale mechanobiology.'

> *(1.4) The larvae studied are about 1 mm long and 0.1 mm in cross-section. Their volumes are therefore on order 0.01 microliter, their masses about 0.01 mg, and their weights in the range of 0.1 micronewton. This contrasts with the force reported for a single protpodium of 1 - 7 micronewtons. This is not to say that the force measurements are incorrect. Larvae crawl easily on an inverted surface, showing gravitational forces are smaller than other forces binding the larva to the substrate. The forces measured in this work are also of the same magnitude as the horizontal forces reported by Khare et al. (ref 32) using micropillar arrays.*
>
> *I suspect that the forces adhering the larva to the substrate are due to the surface tension of a water layer. This would be consistent with the ring of upward stress around the perimeter of the larva visible in S4D, E and in video SV3. The authors remark that upward deflection of the substrate may be due to the Poisson's ratio of the elastomer, but the calibration figure S5 shows that these upward deflections and forces are much smaller than the applied downward force. In any case, there must be a downward force on the larva to balance the measured upward forces and this force must be due to interaction with the substrate. It should be verified that the sum of downward minus upward forces on the gel equals the larva's weight (given the weight is neglible compared to the forces involved, this implies that the upward and downward forces should sum to 0).*

We have carefully calculated the forces exerted by protopodia and are confident in the accuracy of our measurements as reported. We further agree with the reviewer's suggestion that gravitational forces can be largely neglected.

As the reviewer points out, one would expect forces due to upward and downward deflections to cancel when considering the entire system. However, we see indications that the counteracting / balancing force often acts over a much larger area than the acting force, e.g. a sharp indentation by a protopodium might be counteracted by an upward deflection over a 10-20 fold larger radius and hence 100 to 400-fold larger area, thereby reducing the absolute value of the upward deflection at any given pixel surrounding the indentation. This in turn increases error in determining the integrated upward deformation, making it difficult

to perform an absolute comparison of acting and counteracting force. Further, recording the entire counteracting force induced deformation would require acquiring data with a prohibitively large field of view.

We agree that in some situations, water surface tension may be adhering animals to the substrate. Importantly, this is a challenge that the animal faces outside the lab in its natural environment of moist rotting fruit and yeast. The intricate force patterns seen in our study in the presence of water surface tension are therefore ecologically relevant. In other situations (e.g. preparing for pupation), larvae are able to stick to dry surfaces, suggesting that other adhesive forces such as mucoid adhesion can also come into play in certain behavioural contexts. A full characterization of the effects of water tension and mucoid adhesion are beyond the scope of this study. However, we have now added a sentence on pages 8 and 12 commenting on these other biomechanical forces at play:

‘We also observed that the animals travel surrounded by a relatively large water droplet (lines 189-190).’

‘We observed that larvae travel surrounded by moisture from a water droplet, which produces a relatively large upwardly directed force in a ring around the animal. The surface tension produced by such a water droplet likely serves a role in adhering the animal to the substrate. However, during forward waves, we found that protopodia detached completely during SwP, suggesting this surface tensionrelated adhesion force can be easily overcome by the behaving animal. (lines 301-307) .’

> *(1.5) Much of the discussion and the model imply that the sites where the larva exerts downward force on the gel are the sites where horizontal propulsion is generated. This assumption should be justified. Can the authors rule out that the larva 'pulls' itself forward using surface tension instead of 'pushing' itself forward using protopodia?*

Determining the exact ‘sites’ where horizontal propulsion is generated is challenging. In our conceptual model, movement is not initiated by protopodia per se, but rather by a constellation of muscle contractions, which act upon the hydrostatic skeleton, which in turn causes visceral pistoning that heaves larvae forward. This is based on previous findings in Ref 31. While there are indeed downward protopodial ‘vaulting’ forces prior to initiation of swing, we propose that the main function of protopodia is not to push the larvae forward, but rather to provide anchoring to counteract opposing forces generated by muscles. We agree that water surface tension could also be sculpting biomechanical interactions; however, a full characterization of how water surface tension shapes larval locomotion is beyond the scope of this study.

Since we have observed larvae move over dry terrain (e.g. glass) without an encasing water bubble, we do not believe that an encasing water bubble is strictly required for locomotion. We have also seen no obvious locomotion related modulations in the pulling forces created by water bubbles encasing larva, which would be expected if animals were somehow using water tension to pull themselves forward. Overall, the most likely explanation is that larvae use a mixture of biomechanical tactics to suit the moment in a given environment. This represents a challenge but also an opportunity for future research.

We have now added additional text in the ‘Functional subdivisions within protopodia’ subsection to discuss these nuances (page 14, lines 382-387):

‘This increased force transmitted into the substrate is unexpected as the forces generated for the initiation of movement should arise from the contraction of the somatic muscles. We propose that the contraction of the musculature responsible for sequestration acts to move haemolymph into the protopodia thus exerting an increased pressure onto the substrate while the contact area decreases as a consequence of the initiation of sequestration.’

and (page 15, lines 398-399):

'Water surface films appear to facilitate larval locomotion in general but the biomechanical mechanisms by which they do this remain unclear.'

> *(1.6) More detail should be provided about the methods, their limitations, and the rationale behind certain experimental choices.*

We thank the reviewer for this comment. As this significantly overlaps with a point raised earlier, we kindly direct them to our answer to comment #1.2 above.

> *(1.7) Three techniques are introduced here to study how a crawling larva interacts with the substrate: standard brightfield microscopy of a larva crawling in an agarose capillary, ERISM imaging of an immobilized larva, and WARP imaging of a crawling larva. The authors should make clear why each technique was chosen for a particular study - e.g. could the measurements using brightfield microscopy also be accomplished using WARP? They should also clarify how these techniques relate to and possibly improve on existing techniques for measuring forces organisms exert on a substrate, particularly micropillar arrays and Traction Force Microscopy.*

Indeed, each of the three methods used has a specific merit. The brightfield microscopy was selected to track features on the animal's body and to provide a basic control for the later measurements. However, this technique cannot directly measure the substrate interaction, it only allows inferences to be made from tracked features at the substrate interface. ERISM provides high resolution maps of the indentation induced by the larva; it is also extensively validated for mapping cell forces and the data analysis is robust against defects on the substrate (refs 23, 24 and 25). However, as we explain in the manuscript, ERISM lacks the temporal resolution needed to monitor mechanical activity of behaving larva. Its use was therefore limited to the study of anaesthetised animals. For mapping forces exerted by behaving larva, we used WARP which is a further development of ERISM that offers higher frame rates but at the cost of requiring more extensive calibration (Supplementary Figure S4). The streamlined introduction of the different methods in our original manuscript originates from our attempt to be as concise as possible. However, as state in response to comment #1.2, we agree that additional explanation and discussion will be helpful for readers and that it will helpful to briefly refer to other methods for force mapping. We have now added references to a variety of techniques in the Introduction (Page 3-4, lines 56-86) as stated in a prior response.

> *(1.8) As written, "(ERISM) (19) and a variant, Wavelength Alternating Resonance Pressure microscopy (WARP) (20) enable optical mapping of GRFs in the nanonewton range with micrometre and millisecond precision..." (lines 53-55) may generate confusion. ERISM as described in this work has a much lower temporal resolution (requires the animal to be still for 5 seconds - lines 474-5); In this work, WARP does not appear to have nanonewton precision (judging by noise on calibration figures) and it is not clear that it has millisecond precision (the camera used and its frame rate should be specified in the methods).*

Previous studies have demonstrated the capabilities and limitations of ERISM and WARP. Upon reflection, we agree that our wording here could be more precise. To clarify our claim, we now separate the statements on ERISM and WARP in the introduction as follows (page 4, lines 78-83):

"Until recently, this technique was limited by its low temporal resolution (~10s) making it unsuitable for use in recording substrate interaction during fast animal movements, but a

further development of ERISM known as wavelength alternating resonance pressure microscopy (WARP), has been demonstrated to achieve down to 10 ms temporal resolution (26)"

While WARP can achieve comparable force resolution as ERISM when used in a cellular context (c.f. Ref 26), we agree that for the present study, the resolution was in the 10s of nanonewton range, due to the need to use stiffer substrates and larger fields of view.

The camera used in our work was specified in the appropriate subsection of the Materials and Methods ("All WARP and ERISM images were acquired using an Andor Zyla 4.2 sCMOS camera (Andor Technology, Belfast, UK)"). We apologise that the exact frame rate used in our current work was not mentioned in our original manuscript; this has now been added to the 'Freely behaving animals force imaging' section of the Materials and Methods (page 23, lines 574-577).

> *(1.9) It would be helpful to have a discussion of the limits of the techniques presented and tradeoffs that might be involved in overcoming them. For instance, what is the field of view of the WARP microscope, and could it be increased by choosing a lower power objective? What would be required to allow WARP microscopy to measure horizontal forces? Can a crawling larva be imaged over many strides by recentering it in the field of view, or are there only particular regions of the elastomer where a measurement may be made?*

We agree with the reviewer that some discussion of the limitations of our technique will allow readers to have a more informed appreciation of what we are capable of measuring using WARP. However, as this is the first work to ever demonstrate such measurements, the limitations and tradeoffs cannot all be known with certainty at the present stage.

To answer your individual questions:

(1) There is a trade-off between numerical aperture and the ability to resolve individual interference fringes. Since our approach to calculate displacement from reflection maps relies upon counting of individual fringe transitions, going to a lower powered objective risks having these fringes blend and thus the identification of the individual transitions becoming impossible. The minimum numerical aperture of the objective will therefore generally depend on the steepness of indentations produced by the animals; the steeper an indentation, the closer the neighbouring fringes and thus the higher the required magnification to resolve them.

(2) From WARP and ERISM data, one can make inferences about horizontal forces, as is described in detail in our earlier publications about ERISM (ref, 23). However, quantitation of horizontal forces at sufficient temporal resolution to allow the investigation of behaving Drosophila larva is currently not possible.

(3) Many strides can indeed be imaged using our technique, however, this comes with additional technical challenges. Whether or not the animal itself can be recentred is an ongoing challenge. We have found that the animals are amenable to recentring themselves within the field of view if chasing an attractive odorant. However, manual recentering using a paintbrush risks destroying the top surface of the soft elastic resonator and recentering the microscope stage would require real-time object tracking which has been outside the scope of this original work, given the other challenging requirements on hardware and optics for obtaining high quality force maps.

To provide more information on limitations of our technique, we have added the following text into the discussion (pages 13-14, lines 356-370).

‘Despite the substantial advances they have provided, the use of WARP and ERISM also brings challenges and has several technical limitations. For example, fabrication of resonators is much more challenging than preparation of the agarose substrates conventionally used for studying locomotion of Drosophila. This problem is compounded by the fragility of the devices owing to the fragility of the thin gold top mirror. This becomes problematic when placing animals onto the microcavities, as often the area local to the initial placement of the animal is damaged by the paintbrush used to move the animals. Further, as a result of the combining of the two wavelengths, the effective framerate of the resultant displacement and stress maps is equal to half of the recorded framerate of the interference maps. To be able to monitor fast movements, recording at very high framerates is therefore necessary which, depending on hardware, might require imaging at reduced image size, but this in turn reduces the number of peristaltic waves that can be recorded before the animal escapes the field of view. A further limitation is that WARP and ERISM are sensitive mainly to forces in the vertical direction; this is complementary to TFM, which is sensitive to forces in horizontal directions. Using WARP in conjunction with high speed TFM (possibly using the tuneable elastomers presented here) could provide a fully integrated picture of underlying vertical and horizontal traction forces during larval locomotion.’ And further on page 13, lines 337-341:

‘More detailed characterisation of this behaviour remains a challenge owing to the changing position of the mouth hooks. Due to their rigid structure and the relatively large forces produced in planting, mouth hooks produce substrate interaction patterns which our technique struggles to map accurately due to overlapping interference fringes ambiguating the fringe transitions.’

We trust that the above discussion and our modifications to our manuscript resulting from these will address the reviewer’s concerns.

> ***Reviewer #2 (Public Review):***
>
> *(2.1) With a much higher spatiotemporal resolution of ground dynamics than any previous study, the authors uncover new "rules" of locomotory motor sequences during peristalsis and turning behaviors. These new motor sequences will interest the broad neuroscience community that is interested in the mechanisms of locomotion in this highly tractable model. The authors uncover new and intricate patterns of denticle movements and planting that seem to solve the problem of net motion under conditions of force-balance. Simply put, the denticulated "feet" or tail of the Drosophila larva are able to form transient and dynamic anchors that allow other movements to occur.*

We thank the reviewer for their feedback and the information regarding which of our results is likely to resonate most impactfully with readers from a biological background.

> *The biology and dynamics are well-described. The physics is elementary and becomes distracting when occasionally overblown. For example, one doesn't need to invoke Newton's third law, per se, to understand why anchors are needed so that peristalsis can generate forward displacements. This is intuitively obvious.*

We are sorry to hear that the reviewer found some of the physics details distracting. To address this concern, we have simplified some of the language while still attempting to keep the core arguments intact. For context and analogy, we still believe that including a brief reference to the laws of motion is helpful for some readers to explain some of our results and highlight their general implications, especially with regard to anchoring against reaction forces.

One of our objectives is to make this article accessible and interesting for biologists and physicists at all levels. We feel it is important to reach out to both communities and try to be

inclusive as possible in our writing. Newton's 3rd law is clearly relevant for our study and it is a common point of reference for anyone with a highschool education, and so we feel it is appropriate to mention it as a way to help readers across disciplines understand the biophysical challenges faced by the animals we study.

> *(2.2) Another distracting allusion to "physics" is correlating deformation areas with displaced volume, finding that "volume is a consequence of mass in a 2nd order polynomial relationship". I have no idea what this "physics" means or what relevance this relationship has to the biology of locomotion.*

Upon reflection, we agree that this language may be overly complex and distracts from what is, at its core, a simple, but important principle governing how Drosophila larvae interact with their substrates. The point we are trying to make is that our data show that forces exerted by an animal are proportional in a non-linear way to contact area. This suggests that to increase force exerted on the substrate, an animal must increase contact area. We do not observe contact area remaining constant while force increases, or vice versa. To make this result more clear, we have made several changes in our revised manuscript. Figure 5B no longer shows the relationship between the protopodial contact area and the displaced volume of the elastic resonator, but instead now shows the protopodial contact area and recorded force transmitted into the substrate. This then shows that in order to increase force transmitted into the substrate, these animals must increase their contact area. We have made changes to the figure legend of Figure 5 and the statements in the Results section accordingly (Page 9, lines 220-222).

2.3 The ERISM and WARP methods are state-of-the-art, but aside from generally estimating force magnitudes, the detailed force maps are not used. The most important new information is the highly accurate and detailed maps of displacement itself, not their estimates of applied force using finite element calculations. In fact, comparing displacements to stress maps, they are pretty similar (e.g., Fig 4), suggesting that all experiments are performed in a largely linear regime. It should also be noted that the stress maps are assumed to be normal stresses (perpendicular to the plane), not the horizontal stresses that are the ones that actually balance forces in the plane of animal locomotion.

We largely agree with the statement made by the reviewer here. However, we have found that in many contexts, audiences appreciate having the absolute number of the forces and stresses involved reported. Therefore, where possible, we have used stress maps, rather than displacement maps. We also observe that while stress and displacement maps show similar patterns, features sometimes appear sharper in the stress map, which is a result of the finite element algorithm being able to attribute a broad indentation to a somewhat more localised downward force. We have thus opted to keep to original stress maps. We have been more explicit about WARP and ERISM being more tuned to recording vertically directed forces throughout the revised manuscript (lines 75, 78, 86, 162, 301, 305, 336).

We have also modified our Discussion section to encourage further investigation of our proposed model using a technique more tuned to horizontal stresses (pages 12-13, lines 324-328):

'However, WARP microscopy is best suited to measurements of forces in the vertical direction, and though we can make inferences such as this as they are a consequence of fundamental laws of physics, we present this conclusion as a testable prediction which could be confirmed using a force measurement technique more tuned to horizontally directed forces relative to the substrate.'

> *(2.4) But none of this matters. The real achievements are the new locomotory dynamics uncovered with these amazing displacement measurements. I'm only asking the authors*

> *to be precise and down-to-earth about the nature of their measurements.*

We thank the reviewer for their perceptiveness in finding that though the forces are interesting, the interactions themselves are the most noteworthy result here. We trust that with the changes made in our revised manuscript, the description is now more “down-to-earth”, more concise where appropriate, and accurate as to which results are particularly important and novel.

> *(2.5) It would be good to highlight the strength of the paper -- the discovery of new locomotion dynamics with high-resolution microscopy -- by describing it in simple qualitative language. One key discovery is the broad but shallow anchoring of the posterior body when the anterior body undertakes a "head sweep". Another discovery is the tripod indentation at the tail at the beginning of peristalsis cycles.*

We thank the reviewer for this recommendation. We agree that including a more explicit statement of some of our findings, especially with regards to these new posterior tripod structures and the whole-abdomen preparatory anchoring prior to head sweeps, would make the paper more impactful. As a result, we have modified the discussion section to include a statement for each new result and have also amended our abstract as a result (lines 407-416):

“Here we have provided new insights into the behaviour of Drosophila larval locomotion. We have provided new quantitative details regarding the GRFs produced by locomoting larvae with high spatiotemporal resolution. This mapping allowed the first detailed observations of how these animals mitigate friction at the substrate interface and thus provide new rules by which locomotion is achieved. Further, we have ascribed new locomotor function to appendages not previously implicated in locomotion in the form of tripod papillae, providing a new working hypothesis of how these animals initiate movement. These new principles underlying the locomotion outlined here may serve as useful biomechanical constraints as called for by the wider modelling community (39).”

> *(2.6) As far as I know, these anchoring behaviors are new. It is intuitively obvious that anchoring has to occur, but this paper describes the detailed dynamics of anchoring for the first time. Anchoring behavior now has to be included in the motor sequence for Drosophila larva locomotion in any comprehensive biomechanical or neural model.*

We agree with the reviewer on this. We think it is best to let our colleagues reflect on our findings and then decide how best to include them in future models.

> ***Recommendations for the authors:***
>
> ***Reviewer #1 (Recommendations For The Authors):***
>
> *Please be sure to describe in a figure caption or in the methods the details of the optical setup, especially the focal lengths of all the lenses, including the objective, and part numbers of the LEDs and filters. It would be helpful to have a figure in the main paper explaining the principles of ERISM/WARP microscopy along with the calibration measurements and computational pipeline (this would mainly combine elements already in the supplement). Such a figure should also include details of the setup that are alluded to in the methods but not fully explained (for instance, a "silicone well" is referred to in the methods but never described). The calibration of elastomer stiffness that now appears in the main text could be made a supplementary figure, unless there is some new art in the fabrication of the elastomers that should be highlighted as an advance in the main text.*

We appreciate the importance of explaining our methods to readers.

In response to the public comments, we have added further details in our methods section to clarify practical aspects and ensure that readers will be able to reproduce our work.

In Supplemental Figure 2, we show the full optical light path for ERISM and WARP along with named components. In addition, the principles of ERISM and WARP microscopy have already been extensively described in previous publications (See Refs 23-26). In light of this, we feel that the best approach in this paper is to direct readers to those publications.

We feel that it is appropriate to present the calibration of elastomer stiffness in the main text because this is indeed a new innovation that is not just about making the elastomers but making force sensors based on these different materials. This is really important because it shows how researchers can tune the stiffness of an ERISM/WARP elastomer to match the type of tissue or organism under study. This is really the key technical advance that enables whole animal biomechanics across a range of animal sizes, so we think it is appropriate to keep it in the main text.

We want to make sure that we do not oversell this point, and we feel that we make it sufficiently clear in the main text of our manuscript that making elastomer based force sensors of appropriate stiffness is important, when we state

“First, we developed optical microcavities with mechanical stiffnesses in the range found in hydrogel substrates commonly used for studying Drosophila larval behaviour, i.e. Young’s modulus (E) of 10-30kPa (36–38).” (p. 5, ll. 124) and later

“Here we used Drosophila larvae as a test case, but our methods now allow elastic optical resonators to be tuned to a wide range of animal sizes and thus create new possibilities for studying principles of neuro-biomechanics across an array of animals.” (p. 12, ll. 337)

> *I would appreciate a description of the "why" behind some experimental choices, as understanding the motivation would be helpful for other researchers looking to adopt these techniques.*

We have now added additional text in the introduction and discussion that explains the rationale behind our experimental choices. in more detail. Please see our response to Reviewer 1’s public comments on the same point.

> *(1) The WARP and ERISM experiments were conducted on a collagen coated gold surface rather than agarose. Why? EG does agarose not adhere to the gold, or would its thickness interfere with the measurement?*

The gold layer is applied above the elastomer and the collagen on top of the gold layer makes the gold a more natural biological surface for the animals. Agarose is unsuitable as an elastomer because it would dry during the vacuum based deposition of the gold. It is also unsuitable as a surface coating on top of the gold as the coating on the gold needs to very thin to preserve the spatial and mechanical resolution of our sensors. Further, processing of agarose generally requires temperatures of 60°C and higher which we find can damage the elastomer / gold films.

> *(2) The ERISM measurements are made on a cold anesthetized animal right as it starts to wake up (visible mouth-hooks movement), which presents some difficulty. Why not start imaging while the animal is still completely immobile? Or why not use a dead larva?*

This approach allowed us to get measurements of forces exerted by denticles that are physiologically and biomechanically accurate. In dead or fully anesthetized animals, one

cannot be sure that the forces exerted by denticles and denticle bands are representative of the forces exerted by an animal with active hydrostatic control.

> *(3) In the ERISM setup the monochromator is spatially filtered by focusing through pinhole, while in the WARP setup, the LEDs are not.*

Yes that's correct. The LED light sources used in WARP have better spatial homogeneity than the tungsten filament used in ERISM and so a pinhole is not required in WARP.

> *(4) SV4 shows the interference image of a turning larva (presumably from one illumination wavelength) rather than a reconstruction of the displacement or stresses. Why?*

We felt that in this particular case the interference images provided a clearer representation of the behavioural sequence, showing both the small indentations generated by individual denticles and the larger indentations of the animal overall.

> *Lines 49-50 "a lack of methods with sufficient spatiotemporal resolution for measuring GRFs in freely behaving animals has limited progress." This needs a discussion of what sufficient spatial and temporal resolutions would be and how existing methods fall short of these goals.*

We have now rewritten the introduction to include an overview of other alternative approaches and of what we see as the requirements here. See our response to the public comments.

> *Figure caption 1B (line 789) refers to "concave areas of naked cuticle (black line) which generally do not interact with the substrate" While I think this might be supported by later WARP images, it's not clear how the technique of figure 1 measures interaction, which could e.g. be mediated by surface tension of a transparent fluid.*

The technique of Figure 1 provides qualitative information which as the reviewer points out is validated by WARP measurements later.

> *Lines 184-189 "However, unexpectedly, we observed an additional force on the substrate when protopodia leave the substrate (SI) and when they are replanted (ST). To investigate whether this force was due to an active behaviour or due to shifting body mass, we plotted integrated displacement (i.e. displaced volume) against the contact area for each protopodium, combining data from multiple forwards waves (Figure 5B). Area is correlated with displaced volume for most time points, indicating that volume is a consequence of mass in a 2nd order polynomial relationship." I couldn't follow this argument at all.*

We have now reworded this section and explained our rationale. Also see our response to a similar critique in Reviewer 2's public comments.

> *Generally the authors might reconsider their use of acronyms. e.g. (244-246) "SI latencies were much more strongly correlated with wave duration across most segments than ST latencies. SIs scale with SwP and this could be mediated by proprioceptor activity in the periphery" is made more difficult to parse by the abbreviations.*

As we need to refer to these terms multiple times throughout the manuscript, we feel the use of acronyms is appropriate here.

> *The video captions are inadequate. Please expand on them to explain clearly what is shown, and also describe in the methods how the data were acquired and processed. For instance, it seems that in SV3 a motion correction algorithm is applied so that the larva appears stationary even as it crawls forward. I think "fourier filtered" means that the images were processed with a spatial high pass filter - this should be explained and the parameters noted.*

We have revisited the video captions provided in the supplementary information document and conclude that these contain the important information. The mode of acquisition are described in the methods, e.g. Video 1 and 2 see section in Methods on “Denticle band kinematic imaging” and Videos 3 and 4 see section in Methods on WARP. Supplementary Video 3 does not make use of motion correction; indeed, one can see the larvae moving upwards/forwards in the field of view. We apologize for not explaining the Fourier filtering process for Video 3. We have now modified the video caption to read as follows:

Video SV3. WARP imaging during forwards peristalses.

Video showing high frame rate displacement maps produced by a freely behaving Drosophila larva. Displacement maps were Fourier filtered to make denticulated cuticle more readily visible and projected in 3D to show the effects of substrate interaction. Details of the Fourier filtering procedure were described elsewhere [Kronenberg et al, Nat Cell Biol 19, 864–872 (2017)].

> *What were the reflectances of the bottom (10 nm Au/Cr) and top (15nm Au) metal layers at the wavelengths used? I imagine the bottom layer should be less than 38%, the top layer higher, and the product of the square of the bottom transmission and the top reflectance coefficients equal to the bottom reflectance (to make the two paths of the interferometer contribute equal intensity), but none of this is stated.*

The reflectance of the gold mirrors was studied in detail in prior work on ERISM. See Kronenberg et al, Nat Cell Biol 19, 864–872 (2017). We therefore refrained from adding a complete optical characterization of the ERISM sensors again here. In brief, we found that a reflectance >13% at each Au mirror is required for reliable ERISM measurements.

> *The description of the gold coated elastomer as a microcavity is confusing to me. Does the light really make multiple round trips between the plates before returning to the detector? The loss of light on each round trip would depend on the reflectance and parallelism of the top and bottom mirrors. From the WARP calculation it's appears that there is only one round trip - a pi/2 phase shift results from the calculation for one round trip: 2pi*2nL 5nm/(630nm)^2, with n = 1.4 and L = 8 microns - if there were two round trips, the phase shift would be pi etc. Would this better be described as a mostly common path interferometer?*

The physics of our devices is best described within the framework of thin film interference and (weak) microcavity optics. Indeed, light can make multiple roundtrips, though it gets attenuated with each reflection. The complete calculation of the multiple roundtrips is only required to obtain quantitative information on the amount of light that is reflected. The spectral position of minima in reflectance can also be obtained from assuming one roundtrip which is what is done in the description of the WARP calculations.

> *Figure 2 e,f: the line fits appear to be dominated by the data points at 2 s. If these are removed, do the fits change? To support the argument that 2e shows a correlation and 2f does not, some kind of statistical test, ideally a hierarchical bootstrap, should be conducted to compare between the two measurements.*

If we remove the data points at 2 s, then R^2's for swing initiation latencies change as follows: A2: 0.35 to 0.005; A4: 0.78 to 0.31; A6: 0.61 to 0.01. The data in 2e,f are the averages from 3 waves in each animal and so the data points at 2 s are not simply the result of single 'rogue' waves but rather averages of several trials. Further, if all individual waves are plotted, we can see that the overall trends are still visible.

We don't think it is appropriate to remove the data at 2 s from our analysis, but we take the point regarding statements about presence or absence of correlation in a formal sense. We have therefore changed the wording in the description of 2e,f to refer simply to the fact that wave duration can 'largely determine' latencies in some instances, but is less able to in other instances, as is suggested by the R^2 (coefficient of determination) data. In discussion, we have also adjusted our wording.

> *Figure 4 - please provide in the main figure or as a supplement the full images (i.e. not cropped to the assumed shape of the larva)*

We do not feel that it is necessary or helpful to provide the full images given that the focus of the analysis is on dynamics of protopodia movements.

> *Figure 5e top: single data points around wave duration 0.6s appear to dominate fit lines. Does removing these points alter the fits? To support the argument that 5e top shows a correlation and 5e bottom does not, some kind of statistical test, ideally a hierarchical bootstrap, should be conducted to compare between the two measurements.*

In Figure 5e, we are showing all waves analysed across animals. If we remove the datapoints at 0.6 s, A2 R^2 changes from 0.24 to 0.05, A4 R^2 changes from 0.48 to 0.11, A6 R^2 changes from 0.69 to 0.34; however we don't feel it is appropriate to remove these data from our analysis. We take the point about needing to be cautious about making claims about correlation versus no correlation and have now reworded description of these results along same lines as Figure 4.

> *It appears from the methods (467-489) that animals were kept wet for warp imaging but not for ERISM imaging. Please confirm or explain further the presence or absence of a water layer in these two sets of measurements, as this could affect the adhesion forces.*

In each case, the animals were transferred onto experimental substrates with a moistened paintbrush. We have added text explicitly stating this in the methods section.

> *Kim et al. Nature Methods 2017 (10.1038/nmeth.4429) describes recording two images separated by less than 60 microseconds using a scientific CMOS camera with a frame rate of 200 Hz. This is accomplished by triggering a pulsed LED once at the end of one frame's capture window and then a second time at the beginning of the next frame's window (see Supplementary Figure 10). I'm not sure if this trick is widely known, but it's worth considering if the authors are running into a problem with movement between the two wavelength exposures in their WARP setup.*

Thank you for this tip. We will take this under consideration for future work.

> *Is the setup compatible with optogenetics? (EG is the red light dim enough that it wouldn't activate CsChrimson, or could a longer wavelength led be used for interferometry?) If so, activation of mooncrawler descending neuron (MDN) could be used to study backward crawling (or thermogenetic activation of MDN), e.g. to contrast the sites and order of "anchoring" between the two directions of crawling.*

The set-up is potentially compatible with optogenetics. We are in the process of exploring this in current ongoing work.

> ***Reviewer #2 (Recommendations For The Authors):***
>
> *Simplify/reduce the commentary about force measurements, and highlight the clear, qualitative descriptions of the novel locomotion patterns that they have observed. The microscopy and movements seem to matter more than the ground force estimations.*

We have addressed these issues in our responses to Reviewer 2's public comments.